Formulations and Approximations of Branch Flow Model for General Power Networks

Zhao Yuan, *Member*, *IEEE*

***Abstract*—The formulations and approximations of the branch flow model for general (radial and mesh) power networks (General-BranchFlow) are given in this paper. Using different sets of the power flow equations, six formats of the exact General-BranchFlow model are listed. The six formats are mathematically equivalent with each other. Linear approximation and second-order cone programming (SOCP) are then used to derive the six formats of the convex General-BranchFlow model. The branch ampacity constraints considering the shunt conductance and capacitance of the transmission line Π-model are derived. The key foundation of deriving the ampacity constraints is the correct interpretation of the physical meaning of the transmission line Π-model. An exact linear expression of the ampacity constraints of the power loss variable is derived. The applications of the General-BranchFlow model in deriving twelve formats of the exact optimal power flow (OPF) model and twelve formats of the approximate OPF model are formulated and analyzed. Using the Julia programming language, the extensive numerical investigations of all formats of the OPF models show the accuracy and computational efficiency of the General-BranchFlow model. A penalty function based approximation gap reduction method is finally proposed and numerically validated to improve the AC-feasibility of the approximate General-BranchFlow model.**

***Index Terms*—Branch flow, linear approximation, second-order cone programming, ampacity constraint, optimal power flow, radial network, mesh network.**

NOMENCLATURE

A. Sets

$\mathcal{N}, \mathcal{L}$	Sets of nodes (or buses) and lines (or branches)
$\mathcal{C}, \Omega$	Sets of cycles (or closed loops) and decision variables
$\mathcal{N}_n$	Set of nodes with lines directly connected to node n

B. Indices

$n(n'), l$	Indices of nodes and lines

C. Variables

θ_n	Phase-to-ground voltage phase angle at node n
θ_l	Phase angle difference between the sending-end and the receiving-end voltage of branch l
$\theta_{s_l}, \theta_{r_l}$	Sending-end and receiving-end voltage phase angles of branch l
$\theta_{nn'}$	Phase angle difference between nodes n and n'
f	Original objective function
f'	Modified objective function
$K^p_{o_l}, K^q_{o_l}$	Equivalent ampacity constraints for active and reactive power losses
p_n, q_n	Active and reactive power generations at node n
p_{d_n}, q_{d_n}	Active and reactive power demands at node n
p_{gs_l}, q_{bs_l}	Sending-end shunt conductance active power and capacitance reactive power
p_{gr_l}, q_{br_l}	Receiving-end shunt conductance active power and capacitance reactive power
p_{s_l}, q_{s_l}	Non-measurable sending-end active and reactive power flows for branch l
$\tilde{p}_{s_l}, \tilde{q}_{s_l}$	Measurable sending-end active and reactive power flows for branch l
p_{r_l}, q_{r_l}	Non-measurable receiving-end active and reactive power injections of branch l
$\tilde{p}_{r_l}, \tilde{q}_{r_l}$	Measurable receiving-end active and reactive power injections of branch l
v_n, V_n	Phase-to-ground voltage magnitude and voltage square at node n
v_{s_l}, v_{r_l}	Sending-end and receiving-end phase-to-ground voltages of branch l
V_{s_l}, V_{r_l}	Sending-end and receiving-end phase-to-ground voltage squares of branch l

D. Parameters

$\alpha_n, \beta_n, \gamma_n$	Cost parameters of active power generation
$\theta_n^{\min}, \theta_n^{\max}$	Lower and upper bounds of θ_n
$\theta_l^{\min}, \theta_l^{\max}$	Lower and upper bounds of θ_l
$\theta_{nn'}^{\min}, \theta_{nn'}^{\max}$	Lower and upper bounds of $\theta_{nn'}$
ξ	Penalty coefficient
A^+_{nl}, A^-_{nl}	Node-to-line incidence matrices
B_{s_l}, B_{r_l}	Sending-end and receiving-end shunt susceptances of branch l

Manuscript received: September 22, 2021; revised: November 24, 2021; accepted: January 24, 2022. Date of CrossCheck: January 24, 2022. Date of online publication: February 4, 2022.

Z. Yuan (corresponding author) is with the Electrical Power Systems Laboratory (EPS-Lab), Department of Electrical and Computer Engineering, University of Iceland, Reykjavík, Iceland (e-mail: zhaoyuan@hi.is).

DOI: 10.35833/MPCE.2021.000647

G_n, B_n	Shunt conductance and susceptance of node n
$G_{nn'}, B_{nn'}$	Real and imaginary parts of the element in the bus admittance matrix corresponding to the n^{th} row and n'^{th} column
G_{s_l}	Sending-end shunt conductance of branch l
$\tilde{K}_l, K_l$	Actual and approximate ampacities of branch l
p_{d_n}, q_{d_n}	Active and reactive power loads of node n
$p_n^{\min}, p_n^{\max}$	Lower and upper bounds of p_n
$q_n^{\min}, q_n^{\max}$	Lower and upper bounds of q_n
$v_n^{\min}, v_n^{\max}$	Lower and upper bounds of v_n
X_l, R_l	Longitudinal reactance and resistance of branch l modelled as a passive Π-model

I. Introduction

EFFICIENT operations of power systems rely largely on the accurate modeling of power networks and the optimal solutions of the models [1]. Since the first formulation in the year of 1962, the optimal power flow (OPF) model has been investigated in enormous aspects and applied in many areas including operation, planning, control and market clearing [2]-[6]. Reference [7] reports that huge economic benefits, in the scale of billions of US dollars, can be achieved for the global power industry by improving the accuracy or solution quality of the OPF model. A good summary of traditional polar power-voltage, rectangular power-voltage, and rectangular current-voltage formulations of the OPF model can be found in [7]. The large-scale integration of renewable energy resources (RERs) and the growing penetration of distributed energy resources (DERs) are pushing the power system operators to deploy the OPF model with more robust and powerful performance [8], [9]. The recent developments of OPF modeling approaches include second-order cone programming (SOCP), semi-definite programming (SDP), and polynomial optimization [10] - [12]. These approaches convexify the original nonconvex OPF model and thus are useful to find the global optimal solutions which are better than the local optimal solutions obtained from directly solving the original nonconvex OPF model. Compared with the local optimal solutions, the global optimal solutions can provide higher economic gains or engineering benefits. Extensive research efforts have been put to find or prove the conditions of the exactness of the SOCP-based OPF models [13], to ensure the rank-1 solution of the SDP-based OPF models [14] and to improve the computational efficiency of the polynomial optimization based OPF models [15]. The SOCP-based OPF models feature in better computational efficiency compared with the SDP or polynomial optimization based OPF models. This is majorly because the number of variables and constraints of the SOCP-based OPF models is less than those of the SDP or polynomial optimization based OPF models.

The dist-flow branch equations are firstly proposed in [16] to optimally size the capacitors in distribution networks. This formulation is valid only for radial power networks since no voltage phase angle constraints are considered. The voltage phase angle constraints are necessary for mesh power networks according to the Kirchhoff's laws for AC circuits. References [17] and [18] reformulate the dist-flow branch equations in [16] and denote the derived model as branch flow model. For radial power networks, it is proved that the branch flow model in [17] and [18] is valid if there are no upper bounds for the power loads. Though this condition of the power loads to validate the branch flow model in [17] and [18] for radial power networks is not realistic, this work has inspired a vast amount of research efforts to the branch flow model and its applications, for example, in the multi-period optimal gas-power flow (OGPF) problem and in the unbalanced three-phase distribution network context [19], [20]. References [17] and [18] also use SOCP to derive a convex relaxation of the branch flow model. It is shown in [21] - [23] that the ampacity constraint is not fully addressed in the branch flow model derived in [17] and [18]. References [21] - [23] point out that the longitude current variable used in the branch flow model in [17] and [18] is not an actual measurable current according to the physical interpretation of the transmission line Π-model. As an improvement, [21] - [23] formulate an exact optimal flow (OPF) model for radial power networks. Another branch flow model for general power networks (General-BranchFlow) including the voltage phase angle constraint is firstly proposed in [24]. This General-BranchFlow model is then extended, reformulated, and applied in OPF, distribution locational marginal pricing (DLMP), coordination of transmission system operator (TSO) and distribution system operator (DSO), distributed economic dispatch, and super grid coordination [25] - [29]. Reference [26] also proposes a sequential programming method to tighten the relaxation or approximation gap of the General-BranchFlow model. The research work in [30] and [31] shows the applicability of the General-BranchFlow model in the operations of voltage source converter based multi-terminal DC (VSC-MTDC) system and flexible AC transmission system (FACTS). The recent work [32] rigorously proves the relaxation property and accuracy of the reformulated convex General-BranchFlow model. This paper extends the work in [32] to formulate and validate more formats of the General-BranchFlow model, and to derive the transmission line ampacity constraint in a more accurate way.

In this paper, a comprehensive investigation of the six equivalent formats of the exact General-BranchFlow model and the six formats of the approximate General-BranchFlow model is conducted. The work in [32] is extended to derive the ampacity constraints considering both shunt conductive and capacitive components of the transmission line Π-model. Taking the derived ampacity constraints into account, twelve formats of the exact OPF model and twelve formats of the approximate OPF model are formulated based on the General-BranchFlow equations. All the formats of the OPF model are implemented in Julia programming language and the JuMP optimization modeling package [33], [34]. A numerical investigation is then conducted through various IEEE test cases. To improve the accuracy of the approximate General-BranchFlow model, a penalty function based method is proposed and numerically validated. Compared with the work

in [32], the following contributions of this paper are original.

1) This paper provides and investigates six formats of the exact General-BranchFlow model and six formats of the convex General-BranchFlow model. Based on these, twelve formats of the exact OPF model and twelve formats of the convex OPF model are formulated and validated. The previous work [32] only formulates and investigates one format of the convex OPF model.

2) Although all the formats of the exact General-BranchFlow model are mathematically equivalent, their numerical performance can be different for different test cases. This means more models are provided for the power system operators to use, in case one model faces numerical difficulties or parameter non-availability problems in solving network operation problems. The numerical results in this paper confirm this point.

3) For the proposed formats of the General-BranchFlow model, they are not equivalent to each other due to the different approximations or relaxations to the different power network equations. These formats of the convex General-BranchFlow model provide more methods or techniques to find the global optimal solutions of the OPF problem. This point is validated by the numerical results of this paper.

4) This paper considers both shunt conductance and capacitance of the transmission line Π-model. The previous work [32] only considers the shunt capacitance of the transmission line Π-model.

5) This paper proposes and validates a penalty function based method to reduce the approximation gap of the convex OPF models, which is not mentioned in the previous work [32].

6) More numerical examinations of all the poposed formats of the General-BranchFlow model are conducted for the base power loads and heavy power loads conditions. On the contrary, only the base power loads and light power loads for one format of convex OPF model are considered in the previous work [32].

The rest of this paper is organized as follows. Section II presents the General-BranchFlow model including the exact mode, the approximate model, and the branch ampacity constraint. Section III formulates the OPF problem including the exact and approximate OPF models, and provides the numerical validations. Section IV proposes the approximation gap reduction of the approximate General-BranchFlow model by using the penalty function based method, and numerically validates this method. Section V concludes this paper.

II. General-BranchFlow Model

A. Exact Model

It is assumed that the three-phase power network is balanced and the decision variables considered are constrained in (1)-(7).

$$v_n \in (v_n^{\min}, v_n^{\max}) \subseteq (0.9, 1.1) \quad \forall n \in \mathcal{N} \tag{1}$$

$$\theta_n \in (\theta_n^{\min}, \theta_n^{\max}) \subseteq (0, 2\pi) \quad \forall n \in \mathcal{N} \tag{2}$$

$$\theta_l = \theta_{s_l} - \theta_{r_l} \in (\theta_l^{\min}, \theta_l^{\max}) \subseteq \left(-\frac{\pi}{2}, \frac{\pi}{2}\right) \quad \forall l \in \mathcal{L} \tag{3}$$

$$p_n \in (p_n^{\min}, p_n^{\max}) \subset \mathbb{R}^+ \quad \forall n \in \mathcal{N} \tag{4}$$

$$q_n \in (q_n^{\min}, q_n^{\max}) \subset \mathbb{R} \quad \forall n \in \mathcal{N} \tag{5}$$

$$p_{d_n} \in (p_{d_n}^{\min}, p_{d_n}^{\max}) \subset \mathbb{R}^+ \quad \forall n \in \mathcal{N} \tag{6}$$

$$q_{d_n} \in (q_{d_n}^{\min}, q_{d_n}^{\max}) \subset \mathbb{R}^+ \quad \forall n \in \mathcal{N} \tag{7}$$

Note the subscripts s and r in all the relevant variables and parameters $\theta_{s_l}, \theta_{r_l}, v_{s_l}, v_{r_l}, V_{s_l}, p_{s_l}, B_{s_l}, G_{s_l}$ of this paper are not indexes but only to denote the meanings of sending-end and receiving-end. Similar reasoning holds for the subscripts d, o, which are to denote the meaning of demand and power loss in all the relevant variables $p_{d_n}, q_{d_n}, p_{o_l}, q_{o_l}$ of this paper. p_{d_n}, q_{d_n} are taken as variables here to consider possible demand side responses. The demands are equal to fixed values if there is no demand side response. It is assumed that $(v_n^{\min}, v_n^{\max}) \subset (0.9, 1.1)$ in (1) and $(\theta_l^{\min}, \theta_l^{\max}) \subset \left(-\frac{\pi}{2}, \frac{\pi}{2}\right)$ in (3). These assumptions are valid in power system operations under normal conditions.

The nodal power balance equations of the General-BranchFlow model are formulated as:

$$p_n - p_{d_n} = \sum_l (A_{nl}^+ p_{s_l} - A_{nl}^- p_{o_l}) + G_n v_n^2 \quad \forall n \in \mathcal{N} \tag{8}$$

$$q_n - q_{d_n} = \sum_l (A_{nl}^+ q_{s_l} - A_{nl}^- q_{o_l}) - B_n v_n^2 \quad \forall n \in \mathcal{N} \tag{9}$$

Equation (8) represents the active power balance. Equation (9) represents the reactive power balance. A_{nl}^+ and A_{nl}^- are defined as $A_{nl}^+ = 1$, $A_{nl}^- = 0$ if n is the sending-end of branch l, and $A_{nl}^+ = -1$, $A_{nl}^- = -1$ if n is the receiving-end of branch l. The default convention of the sending-end or receiving-end of the lines can be defined in anyway. The only difference is that, the results of the power flow variables p_{s_l}, q_{s_l} from the OPF calculations are negative if the default sending-end or receiving-end is reversed. Figure 1 illustrates this issue. Note that we neglect the power loss in Fig. 1 for sake of simplicity. The default conventions are made before the OPF calculations are done. In convention 1, node n_1 is referred as the sending-end and node n_2 is referred as the receiving-end. A contrary default setting is made in convention 2. In this set-up, after the OPF calculations are done, 100 kW power flow from node n_1 to node n_2 is equivalent to −100 kW power flow from the opposite direction. So the default convention of the sending-end or the receiving-end does not affect the OPF results.

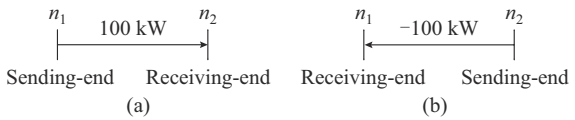

Fig. 1. Different conventions of sending-end and receiving-end of lines. (a) Convention 1. (b) Convention 2.

To relate the power variables $p_{s_l}, q_{s_l}, p_{o_l}, q_{o_l}$ with the voltage variables, the voltage drop phasor of branch l is used to derive the following equations:

$$v_{s_l}^2 - v_{r_l}^2 = 2R_l p_{s_l} + 2X_l q_{s_l} - R_l p_{o_l} - X_l q_{o_l} \quad \forall l \in \mathcal{L} \tag{10}$$

$$v_{s_l} v_{r_l} \sin\theta_l = X_l p_{s_l} - R_l q_{s_l} \quad \forall l \in \mathcal{L} \tag{11}$$

$$v_{s_l}^2 - v_{s_l} v_{r_l} \cos\theta_l = R_l p_{s_l} + X_l q_{s_l} \quad \forall l \in \mathcal{L} \tag{12}$$

where $V_{s_l} = v_{s_l}^2$ and $V_{r_l} = v_{r_l}^2$. According to the proof of Theorem 6 in [32], it is only necessary to use (10), (11) or (11), (12) to sufficiently express the voltage drop phasor. This reasoning is used in listing all the necessary equations of the General-BranchFlow model in Table I.

TABLE I
EXACT GENERAL-BRANCHFLOW MODEL EXPRESSED IN DIFFERENT SETS OF EQUATIONS

Format	Set of equations
1	{(1)-(7)},{(8)-(11)},{(13),(14)}
2	{(1)-(7)},{(8)-(11)},{(13)},{(15)}
3	{(1)-(7)},{(8)-(11)},{(14),(15)}
4	{(1)-(7)},{(8),(9)},{(11),(12)},{(13),(14)}
5	{(1)-(7)},{(8),(9)},{(11),(12)},{(13)},{(15)}
6	{(1)-(7)},{(8),(9)},{(11),(12)},{(14),(15)}

The active power loss and reactive power loss p_{o_l}, q_{o_l} are expressed as:

$$p_{o_l} = \frac{p_{s_l}^2 + q_{s_l}^2}{v_{s_l}^2} R_l \quad \forall l \in \mathcal{L} \tag{13}$$

$$q_{o_l} = \frac{p_{s_l}^2 + q_{s_l}^2}{v_{s_l}^2} X_l \quad \forall l \in \mathcal{L} \tag{14}$$

A linear relationship between p_{o_l} and q_{o_l} exists:

$$p_{o_l} X_l = q_{o_l} R_l \quad \forall l \in \mathcal{L} \tag{15}$$

For mesh power networks, the sum of the phase angles of the voltage drop phasors along each closed network loop $\mathcal{C}$ should satisfy the following cyclic constraint:

$$\sum_{l \in \mathcal{C}} \theta_l = 0 \ mod\ 2\pi \tag{16}$$

As proved and explained in [32], this constraint is implicitly satisfied if θ_l is expressed explicitly using $\theta_{s_l}, \theta_{r_l}$ in constraint (3). So the constraint (16) is not required in the General-BranchFlow model of this paper.

For radial power networks, there are no closed loops. Using $\theta_{s_l}, \theta_{r_l}$ in constraint (3) does not enforce any cyclic constraint which is not necessary for radial power networks.

The exact General-BranchFlow model expressed by selecting different sets of power flow equations is summarized in Table I of this section. The six formats are mathematically equivalent. The exact General-BranchFlow model is valid for both radial and mesh power networks.

B. Approximate Model

Using $V_n = v_n^2$ to replace the voltage magnitude variables, the voltage magnitude bounds (1) can be replaced by:

$$V_n \in (V_n^{\min}, V_n^{\max}) \subseteq (0.81, 1.21) \quad \forall n \in \mathcal{N} \tag{17}$$

Equations (8)-(10) are linearized to [32]:

$$p_n - p_{d_n} = \sum_l (A_{nl}^+ p_{s_l} - A_{nl}^- p_{o_l}) + G_n V_n \quad \forall n \in \mathcal{N} \tag{18}$$

$$q_n - q_{d_n} = \sum_l (A_{nl}^+ q_{s_l} - A_{nl}^- q_{o_l}) - B_n V_n \quad \forall n \in \mathcal{N} \tag{19}$$

$$V_{s_l} - V_{r_l} = 2R_l p_{s_l} + 2X_l q_{s_l} - R_l p_{o_l} - X_l q_{o_l} \quad \forall l \in \mathcal{L} \tag{20}$$

Note the solutions of the original voltage variable v_n can be obtained by $v_n = \sqrt{V_n}$ after solving the approximate General-BranchFlow model.

Equation (11) can be linearized to [32]:

$$\theta_l = X_l p_{s_l} - R_l q_{s_l} \quad \forall l \in \mathcal{L} \tag{21}$$

It is proposed to linearize (12)-(22) in this paper as:

$$\frac{V_{s_l} - V_{r_l}}{2} = R_l p_{s_l} + X_l q_{s_l} \quad \forall l \in \mathcal{L} \tag{22}$$

This linearization is based on the approximation $v_{s_l} v_{r_l} \cos\theta_l \approx (V_{s_l} + V_{r_l})/2$ because $v_{s_l} v_{r_l} \approx (V_{s_l} + V_{r_l})/2$ for $v_n \in (0.9, 1.1)$ and $\theta_l \approx 0$ are valid in power system operations under normal conditions.

Using rotated second-order cone, (13) and (14) can be approximated to:

$$p_{o_l} \geq \frac{p_{s_l}^2 + q_{s_l}^2}{V_{s_l}} R_l \quad \forall l \in \mathcal{L} \tag{23}$$

$$q_{o_l} \geq \frac{p_{s_l}^2 + q_{s_l}^2}{V_{s_l}} X_l \quad \forall l \in \mathcal{L} \tag{24}$$

Note that (20) - (24) are convex since they are rotated cones.

The approximate General-BranchFlow model expressed by selecting different sets of the linearized or convexified power flow equations is summarized in Table II of this section. The six formats are not mathematically equivalent because of the linearizations and approximations of different power flow equations. They are approximate to each other. The approximate General-BranchFlow model is valid for both radial and mesh power networks.

TABLE II
APPROXIMATE GENERAL-BRANCHFLOW MODEL EXPRESSED BY SELECTING DIFFERENT SETS OF EQUATIONS

Format	Set of equations
1	{(2)-(7)},{(17)-(21)},{(23),(24)}
2	{(2)-(7)},{(17)-(21)},{(15)},{(23)}
3	{(2)-(7)},{(17)-(21)},{(15)},{(24)}
4	{(2)-(7)},{(17)-(19)},{(21),(22)},{(23),(24)}
5	{(2)-(7)},{(17)-(19)},{(15)},{(21),(22)},{(23)}
6	{(2)-(7)},{(17)-(19)},{(15)},{(21),(22)},{(24)}

C. Branch Ampacity Constraint

The ampacity constraint of the transmission or distribution line is a very important constraint to avoid over-loading of the corresponding transmission or distribution line. It is important to emphasize the significance of the ampacity constraint considering that several big black-outs such as the Northeast blackout of 2003 in the United States and Canada were caused by the over-loading of transmission lines [35]. This paper extends the previous work [32] to consider both shunt conductance and capacitance of the transmission line

Π-model in deriving the ampacity constraint. Though the shunt conductance is normally very small, it is more accurate to quantify the ampacity constraint by considering this element. The key point here is a correct interpretation of the physical meaning of the transmission line Π-model, i.e., the line-to-ground shunt capacitance and conductance are actually distributed and there is a difference between the actual measurable power flow variables $\tilde{p}_{s_l}, \tilde{q}_{s_l}$ and the power flow variables p_{s_l}, q_{s_l} used in the General-BranchFlow equations. The details about this difference are analyzed in [32]. The transmission line Π-model used in this paper and many other papers in the literature is a lumped representation of the actual line with distributed parameters (resistance, reactance, conductance, and capacitance) by nature. This representation is generally valid for transmission lines above 80 km and below 250 km [1]. Equivalent transmission line Π-model for other line lengths might be derived. Deriving the exact ampacity constraint of the transmission line enables the accurate consideration of its loadability.

From the transmission line Π-model shown in Fig. 2, the following equations can be derived:

$$\tilde{p}_{s_l} = p_{s_l} + p_{gs_l} \tag{25}$$

$$\tilde{q}_{s_l} = q_{s_l} - q_{bs_l} \tag{26}$$

$$p_{gs_l} = V_{s_l} G_{s_l} \tag{27}$$

$$q_{bs_l} = V_{s_l} B_{s_l} \tag{28}$$

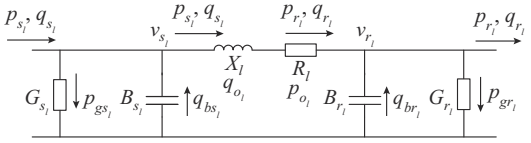

Fig. 2. Transmission line Π-model considering shunt capacitance and conductance.

The branch ampacity constraint is derived as:

$$\left\| \tilde{i}_{s_l} \right\|^2 = \frac{\tilde{p}_{s_l}^2 + \tilde{q}_{s_l}^2}{V_{s_l}} \le \tilde{K}_l \tag{29}$$

The amapcity bound of the transmission line $\tilde{K}_l$ is normally provided by the transmission line manufacturer. $\tilde{q}_{s_l}, \tilde{p}_{s_l}, \tilde{i}_{s_l}$ can be measured from the sending-end of the transmission line. But $q_{s_l}, p_{s_l}, i_{s_l}$ can not be measured because they are physically distributed across the transmission line. From (25)-(29), the gap $\Delta^2 I$ between the current amplitude square $\left\| i_{s_l} \right\|^2$ and the measurable current amplitude square $\left\| \tilde{i}_{s_l} \right\|^2$ in (29) can be formulated as:

$$\begin{aligned} \Delta^2 I = \left\| i_{s_l} \right\|^2 - \left\| \tilde{i}_{s_l} \right\|^2 = \frac{-q_{bs_l}^2 + 2q_{s_l} q_{bs_l} - p_{gs_l}^2 - 2p_{s_l} p_{gs_l}}{V_{s_l}} = \\ \frac{-V_{s_l}^2 B_{s_l}^2 + 2q_{s_l} V_{s_l} B_{s_l}}{V_{s_l}} + \frac{-V_{s_l}^2 G_{s_l}^2 - 2p_{s_l} V_{s_l} G_{s_l}}{V_{s_l}} = \\ -V_{s_l} B_{s_l}^2 + 2q_{s_l} B_{s_l} - V_{s_l} G_{s_l}^2 - 2p_{s_l} G_{s_l} \end{aligned} \tag{30}$$

The branch ampacity constraint (29) is equivalent to:

$$i_{s_l}^2 = \frac{p_{s_l}^2 + q_{s_l}^2}{V_{s_l}} \le K_l = \tilde{K}_l + \Delta^2 I \tag{31}$$

The upper bounds of active power loss and reactive power loss K_{ol}^p, K_{ol}^q can be quantified as:

$$\begin{aligned} K_{o_l}^p = K_l R_l = (\tilde{K}_l + \Delta^2 I) R_l = \\ (\tilde{K}_l - V_{s_l} B_{s_l}^2 + 2q_{s_l} B_{s_l} - V_{s_l} G_{s_l}^2 - 2p_{s_l} G_{s_l}) R_l \end{aligned} \tag{32}$$

$$\begin{aligned} K_{o_l}^q = K_l X_l = (\tilde{K}_l + \Delta^2 I) X_l = \\ (\tilde{K}_l - V_{s_l} B_{s_l}^2 + 2q_{s_l} B_{s_l} - V_{s_l} G_{s_l}^2 - 2p_{s_l} G_{s_l}) X_l \end{aligned} \tag{33}$$

Since G_{s_l} and B_{s_l} are constants, (32) and (33) are linear (the final expressions). The expressions of $K_{o_l}^p$ and $K_{o_l}^q$ from (32) and (33) are used in the exact and approximate General-BranchFlow models. The approximate General-BranchFlow model is still convex. In this way, any approximation on the branch ampacity constraint is avoided. This ampacity constraint can be used to constrain the power loss variable which equivalently constrains the capacity of the transmission lines expressed as:

$$p_{o_l} \le K_{o_l}^p \tag{34}$$

$$q_{o_l} \le K_{o_l}^q \tag{35}$$

III. OPF Problem

The OPF problem is a fundamental mathematical optimization model used widely in power system operations. Power system operators solve the OPF problem to make optimal decisions in the control room. The objective of the decision making can be to minimize the economic generation cost (economic dispatch), to minimize the power loss or maximize the security margin, etc. Any decisions in operating the power network must take into account physical laws of power flow and various operational constraints. In this paper, $\Omega \subseteq \{p_n, q_n, p_{d_n}, q_{d_n}, v_n, V_n, \theta_l, p_{s_l}, q_{s_l}, p_{o_l}, q_{o_l}\}$ is used to represent the set of decision variables in expressing the OPF model. For ease of the comparison with the proposed OPF model in this paper, the original OPF formulation in the polar format is re-stated as the objective function (36) subject to constraints (1), (2), (4)-(7), and (37)-(39).

$$\min f = f(\Omega) \tag{36}$$

$$p_n - p_{d_n} = v_n \sum_{n' \in \mathcal{N}_n} v_{n'} (G_{nn'} \cos\theta_{nn'} + B_{nn'} \sin\theta_{nn'}) \quad \forall n \in \mathcal{N} \tag{37}$$

$$q_n - q_{d_n} = v_n \sum_{n' \in \mathcal{N}_n} v_{n'} (G_{nn'} \sin\theta_{nn'} - B_{nn'} \cos\theta_{nn'}) \quad \forall n \in \mathcal{N} \tag{38}$$

$$\theta_{nn'} \in (\theta_{nn'}^{\min}, \theta_{nn'}^{\max}) \quad \forall n, n' \in \mathcal{N} \tag{39}$$

where $n' \in \mathcal{N}$ is the alias of n. Equation (37) is the active power balance equation; (38) is the reactive power balance equation; and $\theta_{nn'} = \theta_n - \theta_{n'}$.

By deploying one format of the exact General-BranchFlow model in Table I or the approximate General-BranchFlow model in Table II as the constraints of the OPF problem, different formats of the exact OPF problem or the ap-

proximate OPF problem can be formulated. For the branch ampacity constraint, either constraints (32)-(34) or (33)-(35) described in the Section II of this paper can be used. Twelve formats of the exact OPF model are listed in Table III. They are mathematically equivalent.

TABLE III
FORMATS OF EXACT OPF MODEL

Format	Exact OPF Model
1	$\underset{\Omega}{\text{argmin}}\ f(\Omega):=\{\Omega\in\{(1)\text{-}(7)\},\{(8)\text{-}(11)\},\{(13),(14)\},\{(32)\},\{(34)\}\}$
2	$\underset{\Omega}{\text{argmin}}\ f(\Omega):=\{\Omega\in\{(1)\text{-}(7)\},\{(8)\text{-}(11)\},\{(13)\},\{(15)\},\{(32)\},\{(34)\}\}$
3	$\underset{\Omega}{\text{argmin}}\ f(\Omega):=\{\Omega\in\{(1)\text{-}(7)\},\{(8)\text{-}(11)\},\{(14),(15)\},\{(32)\},\{(34)\}\}$
4	$\underset{\Omega}{\text{argmin}}\ f(\Omega):=\{\Omega\in\{(1)\text{-}(7)\},\{(8),(9)\},\{(11),(12)\},\{(13),(14)\},\{(32)\},\{(34)\}\}$
5	$\underset{\Omega}{\text{argmin}}\ f(\Omega):=\{\Omega\in\{(1)\text{-}(7)\},\{(8),(9)\},\{(11),(12)\},\{(13)\},\{(15)\},\{(32)\},\{(34)\}\}$
6	$\underset{\Omega}{\text{argmin}}\ f(\Omega):=\{\Omega\in\{(1)\text{-}(7)\},\{(8),(9)\},\{(11),(12)\},\{(14),(15)\},\{(32)\},\{(34)\}\}$
7	$\underset{\Omega}{\text{argmin}}\ f(\Omega):=\{\Omega\in\{(1)\text{-}(7)\},\{(8)\text{-}(11)\},\{(13),(14)\},\{(33)\},\{(35)\}\}$
8	$\underset{\Omega}{\text{argmin}}\ f(\Omega):=\{\Omega\in\{(1)\text{-}(7)\},\{(8)\text{-}(11)\},\{(13)\},\{(15)\},\{(33)\},\{(35)\}$
9	$\underset{\Omega}{\text{argmin}}\ f(\Omega):=\{\Omega\in\{(1)\text{-}(7)\},\{(8)\text{-}(11)\},\{(14),(15)\},\{(33)\},\{(35)\}\}$
10	$\underset{\Omega}{\text{argmin}}\ f(\Omega):=\{\Omega\in\{(1)\text{-}(7)\},\{(8),(9)\},\{(11),(12)\},\{(13),(14)\},\{(33)\},\{(35)\}\}$
11	$\underset{\Omega}{\text{argmin}}\ f(\Omega):=\{\Omega\in\{(1)\text{-}(7)\},\{(8),(9)\},\{(11),(12)\},\{(13)\},\{(15)\},\{(33)\},\{(35)\}\}$
12	$\underset{\Omega}{\text{argmin}}\ f(\Omega):=\{\Omega\in\{(1)\text{-}(7)\},\{(8),(9)\},\{(11),(12)\},\{(14),(15)\},\{(33)\},\{(35)\}\}$

To improve the AC-feasibility of the approximate General-BranchFlow model, the following conic constraint (40) is proven to be a necessary condition to recover the AC-feasible solution [32]:

$$V_{s_l}V_{r_l}\sin^2(\theta_l^{\max})\geq\theta_l^2\quad\forall l\in\mathcal{L} \tag{40}$$

This constraint is included in the approximate OPF model based on the approximate General-BranchFlow equations. Since this constraint is conic, it is convex. Twelve formats of the approximate OPF model are listed in Table IV. They are not mathematically equivalent but are approximate to each other.

For the approximate OPF model, the approximation gaps of active power loss gap_l^{po} and reactive power loss gap_l^{qo} are defined as:

$$gap_l^{po}:=\left|p_{o_l}-\frac{p_{s_l}^2+q_{s_l}^2}{V_{s_l}}R_l\right|\quad\forall l\in\mathcal{L} \tag{41}$$

$$gap_l^{qo}:=\left|q_{o_l}-\frac{p_{s_l}^2+q_{s_l}^2}{V_{s_l}}X_l\right|\quad\forall l\in\mathcal{L} \tag{42}$$

TABLE IV
FORMATS OF APPROXIMATE OPF MODEL

Format	Approximate OPF model
1	$\underset{\Omega}{\text{argmin}}\ f(\Omega):=\{\Omega\in\{(2)\text{-}(7)\},\{(17)\text{-}(21)\},\{(23),(24)\},\{(32)\},\{(34)\},\{(40)\}\}$
2	$\underset{\Omega}{\text{argmin}}\ f(\Omega):=\{\Omega\in\{(2)\text{-}(7)\},\{(17)\text{-}(21)\},\{(15)\},\{(23)\},\{(32)\},\{(34)\},\{(40)\}\}$
3	$\underset{\Omega}{\text{argmin}}\ f(\Omega):=\{\Omega\in\{(2)\text{-}(7)\},\{(17)\text{-}(21)\},\{(15)\},\{(24)\},\{(32)\},\{(34)\},\{(40)\}\}$
4	$\underset{\Omega}{\text{argmin}}\ f(\Omega):=\{\Omega\in\{(2)\text{-}(7)\},\{(17)\text{-}(19)\},\{(21),(22)\},\{(23),(24)\},\{(32)\},\{(34)\},\{(40)\}\}$
5	$\underset{\Omega}{\text{argmin}}\ f(\Omega):=\{\Omega\in\{(2)\text{-}(7)\},\{(17)\text{-}(19)\},\{(15)\},\{(21),(22)\},\{(23)\},\{(32)\},\{(34)\},\{(40)\}\}$
6	$\underset{\Omega}{\text{argmin}}\ f(\Omega):=\{\Omega\in\{(2)\text{-}(7)\},\{(17)\text{-}(19)\},\{(15)\},\{(21),(22)\},\{(24)\},\{(32)\},\{(34)\},\{(40)\}\}$
7	$\underset{\Omega}{\text{argmin}}\ f(\Omega):=\{\Omega\in\{(2)\text{-}(7)\},\{(17)\text{-}(21)\},\{(23),(24)\},\{(33)\},\{(35)\},\{(40)\}\}$
8	$\underset{\Omega}{\text{argmin}}\ f(\Omega):=\{\Omega\in\{(2)\text{-}(7)\},\{(17)\text{-}(21)\},\{(15)\},\{(23)\},\{(33)\},\{(35)\},\{(40)\}\}$
9	$\underset{\Omega}{\text{argmin}}\ f(\Omega):=\{\Omega\in\{(2)\text{-}(7)\},\{(17)\text{-}(21)\},\{(15)\},\{(24)\},\{(33)\},\{(35)\},\{(40)\}\}$
10	$\underset{\Omega}{\text{argmin}}\ f(\Omega):=\{\Omega\in\{(2)\text{-}(7)\},\{(17)\text{-}(19)\},\{(21),(22)\},\{(23),(24)\},\{(33)\},\{(35)\},\{(40)\}\}$
11	$\underset{\Omega}{\text{argmin}}\ f(\Omega):=\{\Omega\in\{(2)\text{-}(7)\},\{(17)\text{-}(19)\},\{(15)\},\{(21),(22)\},\{(23)\},\{(33)\},\{(35)\},\{(40)\}\}$
12	$\underset{\Omega}{\text{argmin}}\ f(\Omega):=\{\Omega\in\{(2)\text{-}(7)\},\{(17)\text{-}(19)\},\{(15)\},\{(21),(22)\},\{(24)\},\{(33)\},\{(35)\},\{(40)\}\}$

The corresponding maximum approximation gaps (of active and reactive power losses) are defined as:

$$gap^{po,\max}:=\max\left\{gap_l^{po},\ \forall l\in\mathcal{L}\right\} \tag{43}$$

$$gap^{qo,\max}:=\max\left\{gap_l^{qo},\ \forall l\in\mathcal{L}\right\} \tag{44}$$

These approximation gaps are useful to quantify the AC-feasibility of the solutions from the approximate OPF model. A fully AC-feasible solution of the approximate OPF model means that $gap^{po,\max}=gap^{qo,\max}=0$. When $gap^{po,\max}\neq 0$ or $gap^{qo,\max}\neq 0$, smaller values of $gap^{po,\max}, gap^{qo,\max}$ mean better solution quality in terms of AC-feasibility.

A typical example of the OPF problem to minimize a quadratic power generation cost function as the objective function f is formulated in (45). This formulation is also used in the OPF formulations in MATPOWER, which is a benchmark OPF software package based on MATLAB.

$$f(p_n)=\sum_n(\alpha_n p_n^2+\beta_n p_n+\gamma_n) \tag{45}$$

where $\alpha_n,\beta_n,\gamma_n\geq 0$. Numerical investigations of the OPF model using (45) as the objective function are conducted in this section.

All the formats of the OPF model listed in Table III and Table IV are implemented in the Julia programming language and the JuMP optimization modeling package. The codes are running on the 64-bit Windows 10 operating system. A personal computer with Intel-i7 3 GHz CPU and 32 GB RAM is deployed. The IPOPT solver is used to solve the exact OPF model and the approximate OPF model in Julia [36]. Some test cases of the approximate OPF model are solved by the CPLEX solver. The power network data (including the cost parameters $\alpha_n, \beta_n, \gamma_n$) from MATPOWER is used here [37]. The evaluated power networks include case9, IEEE14, case30, IEEE57, case89pegase, IEEE118, IEEE300, ACTIVSg200, and ACTIVSg500 [38]-[41]. The OPF solutions from MATPOWER are used as the benchmark. Note that even the test cases used in this paper are mesh power networks, while there are many radial branches in these power networks. For example, in Fig. 3, one sub-network in radial topology is shown for the IEEE300 test case. These radial branches can be regarded as sub-networks in radial topology. In other words, the numerical results in this paper validate the OPF models for both radial and mesh power networks.

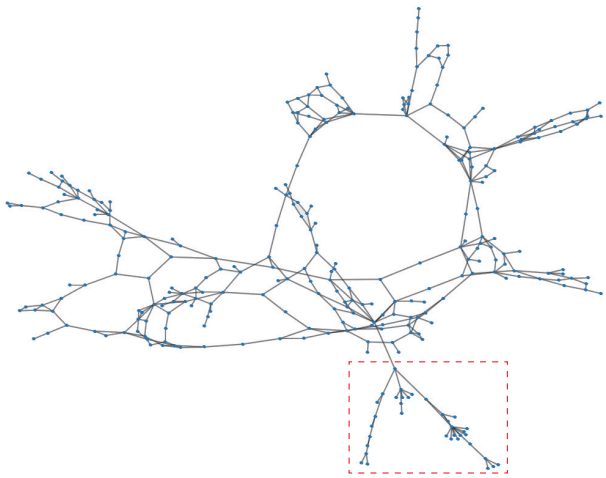

Fig. 3. Network topology of IEEE300 test case.

A. Base Power Loads

The performance of the proposed OPF models for the base power loads is examined in this subsection. The base power loads are equal to the original power loads according to the test case data in MATPOWER.

The objective solutions of the exact OPF model are listed in Table V. All the proposed twelve formats of the exact OPF model have the same or very close objective solutions compared with MATPOWER. These results show that all the proposed formats of the exact OPF model are accurate. The computational CPU time of the exact OPF model are listed in Table VI. Note that the computational time for the proposed twelve formats of the OPF model includes both optimization model construction time in JuMP and the solver time in IPOPT.

TABLE V
OBJECTIVE SOLUTIONS OF EXACT OPF MODEL FOR BASE POWER LOADS

Format	Objective solution ($)								
	case9	IEEE14	case30	IEEE57	case89pegase	IEEE118	ACTIVSg200	IEEE300	ACTIVSg500
1	5296.69	8081.61	576.89	41738.11	5819.69	129660.63	27557.57	719732.11	71817.42
2	5314.02	8078.80	573.94	41698.64	5814.88	129695.30	27557.57	719377.57	71817.42
3	5296.69	8081.61	576.89	41738.11	5819.69	129660.63	27557.57	719732.11	71817.42
4	5296.69	8081.54	576.89	41737.93	5819.51	129660.54	27557.57	719732.22	71817.42
5	5296.68	8080.11	576.21	41696.02	5831.56	129930.62	27557.57	719396.40	71817.42
6	5296.69	8081.54	576.89	41737.93	5819.51	129660.54	27557.57	719731.22	71817.42
7	5296.69	8081.61	576.89	41738.11	5819.69	129660.63	27557.57	719732.11	71817.42
8	5296.68	8078.80	577.77	41698.64	5849.61	129695.30	27557.57	719377.57	71817.42
9	5296.69	8081.61	576.89	41738.11	5819.69	129660.63	27557.57	719732.11	71817.42
10	5296.69	8081.54	576.89	41737.93	5819.51	129660.54	27557.57	719731.22	71817.42
11	5309.00	8080.12	578.38	41696.02	5824.01	129930.62	27557.57	719396.40	71817.42
12	5296.69	8081.54	576.89	41737.93	5819.51	129660.54	27557.57	719731.22	71817.42
MATPOWER	5296.69	8081.53	576.89	41737.79	5819.81	129660.70	27557.57	719725.11	72578.30

With the increase of the network scale, the required computational CPU time increases. This is reasonable since the number of model variables and constraints increases. It can also be observed that, in some test cases, the computational time of one specific format of the OPF model is very different from the other formats. This is majorly because of the different formulations or constraints in different formats of the OPF model. These results also demonstrate the advantages of providing more formats of the OPF models to give power system operators more options in modeling and solving network operation problems. In other words, if one format of OPF models faces the numerical inefficiency problem for a specific power network, another format can be used.

The objective solutions of the approximate OPF model are listed in Table VII. The proposed twelve formats of the approximate OPF model have slightly different objective solutions due to the approximations of different constraints and the different selection of the constraints. The computational time of the approximate OPF model is listed in Table VIII. Note that the computational time for the proposed twelve for-

mats of the approximate OPF model includes both optimization model construction time in JuMP and the solver time in IPOPT. Similarly, with the increase of the network scale, the required computational CPU time increases. This is reasonable since the numbers of model variables and constraints increase. Compared with the computational time of the exact OPF model, when the IPOPT solver converges, the required computational time of the approximate OPF model is more or less the same. The non-uniformity of the computational time listed in Table VIII is majorly because of the different network parameters in the test cases. For example, in the test case of IEEE300, some transmission lines have negative reactance values which is the major cause of the non-uniformity of the computational time.

TABLE VI
COMPUTATIONAL TIME OF EXACT OPF MODEL FOR BASE POWER LOADS

Format	Computational time (s)								
	case9	IEEE14	case30	IEEE57	case89pegase	IEEE118	ACTIVSg200	IEEE300	ACTIVSg500
1	0.03	0.02	0.05	0.08	0.33	0.27	0.63	0.95	1.67
2	0.16	0.03	0.08	0.14	5.20	1.36	0.59	2.33	1.64
3	0.05	0.02	0.06	0.06	0.33	0.27	0.83	0.88	1.64
4	0.03	0.02	0.06	0.08	0.27	0.25	0.66	0.98	1.77
5	0.33	0.03	0.31	0.13	3.56	0.81	0.86	1.36	1.72
6	0.03	0.02	0.06	0.06	0.36	0.24	0.86	0.95	1.70
7	0.05	0.03	0.09	0.08	0.22	0.25	0.59	0.95	2.66
8	0.94	0.03	0.52	0.13	2.80	1.36	0.56	2.12	5.02
9	0.05	0.03	0.06	0.08	0.20	0.25	0.55	0.91	2.94
10	0.05	0.02	0.06	0.06	0.22	0.25	0.61	1.02	2.77
11	1.61	0.03	5.06	0.11	3.41	0.83	0.55	1.34	3.94
12	0.05	0.03	0.06	0.06	0.22	0.27	0.56	0.95	3.33
MATPOWER	1.20	1.67	2.14	1.88	2.50	2.02	2.09	2.13	2.78

TABLE VII
OBJECTIVE SOLUTIONS OF APPROXIMATE OPF MODEL FOR BASE POWER LOADS

Format	Objective solution ($)								
	case9	IEEE14	case30	IEEE57	case89pegase	IEEE118	ACTIVSg200	IEEE300	ACTIVSg500
1	5296.69	8080.44	575.33	41734.92	5814.56	129618.44	27553.67	719596.69	71891.92
2	5296.69	8080.64	576.51	41728.82	5819.04	129625.35	27557.57	719548.84	71893.41
3	5296.69	8081.55	576.85	41735.91	5819.05	129626.18	27557.57	719699.91	71893.41
4	5296.49	8081.97	575.68	41726.41	5813.30	129606.68	27553.70	719710.59	71930.49
5	5315.48	8081.43	576.28	41719.61	5816.87	129614.02	27557.58	719456.87	71931.89
6	5315.49	8081.97	576.29	41726.41	5816.87	129615.15	27557.58	719824.73	71931.89
7	5296.69	8080.44	576.66	41734.92	5815.25	129618.44	27553.79	719596.69	71891.99
8	5296.69	8080.64	576.51	41728.82	5819.04	129625.35	27557.57	719548.84	71893.42
9	5296.69	8081.55	576.85	41735.91	5819.05	129626.18	27557.57	719699.91	71893.42
10	5315.49	8081.97	576.15	41726.41	5813.30	129606.68	27553.70	719710.59	71930.49
11	5315.48	8081.43	576.28	41719.61	5816.87	129614.02	27557.58	719456.87	71931.89
12	5315.49	8081.97	576.29	41726.41	5816.87	129615.15	27557.58	719824.73	71931.89

The results of the maximum approximation gaps of active power loss of the approximate OPF model are listed in Table IX. Most values are very small or negligible. The results of the maximum approximation gaps of reactive power loss of the approximate OPF model are listed in Table X. Most of these values are larger compared with those of the maximum approximation gaps of active power loss listed in Table IX. Comparing the results of objective solutions in Table V and Table VII, most of the objective solutions of the convex OPF models are lower than the corresponding objective solutions of the original nonconvex OPF models. This means the convex OPF models can find the lower bounds of the objective solution in most cases. When the relaxation (approximation) gap is zero, the solutions from the convex OPF models are global optimal for the corresponding test cases. For example, for the test cases of ACTIVSg200, the relaxation (approximation) gaps of most formats of the convex OPF models are almost equal to 0 (below 10^{-9}). In other words, the solutions of these test cases from the convex OPF models are globally optimal. For the test cases with non-zero or large relaxation (approximation) gaps, a method to reduce the approximation gaps is proposed and validated in the next section.

TABLE VIII
COMPUTATIONAL TIME OF APPROXIMATE OPF MODEL FOR BASE POWER LOADS

Format	Computational time (s)								
	case9	IEEE14	case30	IEEE57	case89pegase	IEEE118	ACTIVSg200	IEEE300	ACTIVSg500
1	0.03	0.05	0.09	0.16	0.56	0.48	0.77	1.49	2.83
2	0.05	0.05	0.16	0.31	1.08	0.80	0.64	4.06	2.27
3	0.03	0.03	0.08	0.11	0.41	0.33	0.62	1.38	2.13
4	0.03	0.05	0.13	0.16	1.00	0.44	0.78	1.56	2.89
5	0.06	0.06	0.09	0.28	0.41	0.94	0.72	5.67	2.25
6	0.03	0.03	0.06	0.14	0.41	0.38	0.69	1.75	2.19
7	0.03	0.05	0.09	0.16	0.53	0.45	0.72	1.77	3.17
8	0.05	0.05	0.08	0.28	0.83	0.80	0.69	4.00	4.47
9	0.03	0.03	0.08	0.11	0.37	0.33	0.66	1.49	3.31
10	0.03	0.05	0.13	0.14	0.52	0.42	0.78	1.75	2.69
11	0.06	0.05	0.05	0.26	1.00	0.91	0.69	5.42	2.34
12	0.05	0.03	0.09	0.11	0.41	0.34	0.67	1.88	2.25

TABLE IX
THE MAXIMUM APPROXIMATION GAP OF ACTIVE POWER LOSS OF APPROXIMATE OPF MODEL FOR BASE POWER LOADS

Format	The maximum approximation gap								
	case9	IEEE14	case30	IEEE57	case89pegase	IEEE118	ACTIVSg200	IEEE300	ACTIVSg500
1	0.00×10^{0}	0.00×10^{0}	0.00×10^{0}	0.00×10^{0}	2.53×10^{-11}	0.00×10^{0}	2.01×10^{-12}	5.15×10^{-14}	7.11×10^{-14}
2	7.70×10^{-14}	1.29×10^{-10}	5.39×10^{-15}	8.00×10^{-11}	1.85×10^{-2}	2.54×10^{-12}	3.49×10^{-12}	2.84×10^{-13}	2.95×10^{-15}
3	0.00×10^{0}	0.00×10^{0}	0.00×10^{0}	0.00×10^{0}	1.85×10^{-2}	0.00×10^{0}	3.49×10^{-12}	3.39×10^{-14}	2.95×10^{-15}
4	0.00×10^{0}	0.00×10^{0}	0.00×10^{0}	0.00×10^{0}	2.53×10^{-11}	0.00×10^{0}	3.42×10^{-13}	5.60×10^{-14}	7.06×10^{-14}
5	3.02×10^{-13}	1.30×10^{-10}	8.23×10^{-15}	7.85×10^{-11}	1.61×10^{-2}	2.95×10^{-12}	2.09×10^{-12}	4.38×10^{-3}	3.42×10^{-14}
6	0.00×10^{0}	0.00×10^{0}	0.00×10^{0}	0.00×10^{0}	1.61×10^{-2}	0.00×10^{0}	2.09×10^{-12}	4.32×10^{-3}	3.42×10^{-14}
7	0.00×10^{0}	0.00×10^{0}	0.00×10^{0}	0.00×10^{0}	2.53×10^{-11}	0.00×10^{0}	2.01×10^{-12}	5.15×10^{-14}	7.11×10^{-14}
8	7.06×10^{-11}	1.29×10^{-10}	2.14×10^{-8}	8.00×10^{-11}	1.85×10^{-2}	2.54×10^{-12}	3.49×10^{-12}	2.84×10^{-13}	2.95×10^{-15}
9	0.00×10^{0}	0.00×10^{0}	0.00×10^{0}	0.00×10^{0}	1.85×10^{-2}	0.00×10^{0}	3.49×10^{-12}	3.39×10^{-14}	2.95×10^{-15}
10	0.00×10^{0}	0.00×10^{0}	0.00×10^{0}	0.00×10^{0}	2.53×10^{-11}	0.00×10^{0}	2.01×10^{-12}	5.60×10^{-14}	7.06×10^{-14}
11	7.06×10^{-11}	1.30×10^{-10}	4.11×10^{-9}	7.85×10^{-11}	1.61×10^{-2}	2.95×10^{-12}	2.09×10^{-12}	4.38×10^{-3}	3.42×10^{-14}
12	0.00×10^{0}	0.00×10^{0}	0.00×10^{0}	0.00×10^{0}	1.61×10^{-2}	0.00×10^{0}	2.09×10^{-12}	4.32×10^{-3}	3.42×10^{-14}

TABLE X
THE MAXIMUM APPROXIMATION GAP OF REACTIVE POWER LOSS OF APPROXIMATE OPF MODEL FOR BASE POWER LOADS

Format	The maximum approximation gap								
	case9	IEEE14	case30	IEEE57	case89pegase	IEEE118	ACTIVSg200	IEEE300	ACTIVSg500
1	3.32×10^{-1}	2.43×10^{-1}	3.08×10^{-1}	1.25×10^{-1}	3.47×10^{0}	6.02×10^{0}	4.84×10^{-1}	3.13×10^{0}	2.98×10^{-1}
2	2.40×10^{-1}	4.63×10^{-10}	6.14×10^{-2}	1.14×10^{-1}	1.47×10^{0}	3.99×10^{0}	2.55×10^{-10}	1.00×10^{0}	3.35×10^{-13}
3	3.32×10^{-1}	4.07×10^{-10}	8.49×10^{-2}	8.30×10^{-2}	1.47×10^{0}	4.23×10^{0}	2.55×10^{-10}	8.14×10^{-1}	3.35×10^{-13}
4	2.07×10^{0}	2.13×10^{-1}	2.61×10^{-1}	4.75×10^{-1}	2.15×10^{0}	7.42×10^{0}	3.20×10^{-1}	2.27×10^{4}	1.01×10^{-1}
5	1.71×10^{0}	8.65×10^{-2}	1.75×10^{-1}	1.47×10^{-1}	1.27×10^{0}	2.96×10^{0}	1.52×10^{-10}	1.00×10^{5}	3.88×10^{-12}
6	2.12×10^{0}	9.58×10^{-2}	2.18×10^{-1}	1.44×10^{-1}	1.27×10^{0}	3.45×10^{0}	1.52×10^{-10}	1.05×10^{4}	3.88×10^{-12}
7	2.41×10^{-1}	2.43×10^{-1}	9.89×10^{-2}	1.25×10^{-1}	1.53×10^{0}	6.02×10^{0}	3.69×10^{-1}	3.13×10^{0}	1.52×10^{-1}
8	1.41×10^{-1}	4.63×10^{-10}	1.30×10^{-2}	1.14×10^{-1}	1.44×10^{0}	3.99×10^{0}	2.55×10^{-10}	1.00×10^{0}	3.35×10^{-13}
9	2.41×10^{-1}	4.07×10^{-10}	2.63×10^{-2}	8.30×10^{-2}	1.47×10^{0}	4.23×10^{0}	2.55×10^{-10}	8.14×10^{-1}	3.35×10^{-13}
10	1.85×10^{-1}	2.13×10^{-1}	9.69×10^{-2}	4.75×10^{-1}	2.15×10^{0}	7.42×10^{0}	5.42×10^{-1}	2.27×10^{4}	1.53×10^{-1}
11	1.01×10^{-1}	8.65×10^{-2}	3.28×10^{-2}	1.47×10^{-1}	1.27×10^{0}	2.96×10^{0}	1.52×10^{-10}	1.00×10^{5}	3.88×10^{-12}
12	1.85×10^{-1}	9.58×10^{-2}	9.78×10^{-2}	1.44×10^{-1}	1.27×10^{0}	3.45×10^{0}	1.52×10^{-10}	1.05×10^{4}	3.88×10^{-12}

B. Heavy Power Loads

The performance of the proposed OPF models for the heavy power loads is examined in this subsection. The heavy power loads are obtained by increasing the original

power loads at all the nodes of the test case data from MATPOWER. The heavy power loads range from 110% to 200% (with a gradual increment of 10%) of the base power loads. Since the IPOPT solver can find all the optimal solutions in heavy power loads for the case9 and IEEE118 in MATPOWER, we list all results for the proposed formats of the OPF models for case9 and IEEE118.

The objective solutions of the exact OPF model for heavy power loads of case9 are listed in Table XI. The computational time of the exact OPF model for heavy power loads of case9 is listed in Table XII. The objective solutions of the exact OPF model for heavy power loads of IEEE118 are listed in Table XIII. The computational time of the exact OPF model for heavy power loads of IEEE118 is listed in Table XIV. The objective solutions of the approximate OPF model for heavy power loads of case9 are listed in Table XV. The computational time of the exact OPF model for heavy power loads of case9 is listed in Table XVI. The maximum approximation gaps of the active power loss of the approximate OPF model for the heavy power loads of case9 are listed in Table XVII. The maximum approximation gaps of the reactive power loss of the approximate OPF model for the heavy power loads of case9 are listed in Table XVIII. The objective solutions of the approximate OPF model for heavy power loads of IEEE118 are listed in Table XIX. The computational time of the exact OPF model for heavy power loads of IEEE118 is listed in Table XX. The maximum approximation gaps of the active power loss of the approximate OPF model for the heavy power loads of IEEE118 are listed in Table XXI. The maximum approximation gaps of the reactive power loss of the approximate OPF model for the heavy power loads of IEEE118 are listed in Table XXII. These results show that the proposed OPF models based on the General-BranchFlow equations in this paper are robust in terms of the power loads, which can force the decision variables or line capacities to the limits. In most cases, the computational efficiency of the proposed OPF models executed in Julia outperforms MATPOWER.

TABLE XI
OBJECTIVE SOLUTIONS OF EXACT OPF MODEL FOR HEAVY POWER LOADS OF CASE9

Format	Objective solution ($)									
	110%	120%	130%	140%	150%	160%	170%	180%	190%	200%
1	6114.27	7006.02	7972.52	9014.71	10133.71	11330.27	12605.50	13960.63	15397.09	16916.52
2	6114.03	7004.97	7982.45	9013.78	10127.29	11384.69	12583.93	13938.51	15452.18	16970.22
3	6114.27	7006.02	7972.52	9014.71	10133.71	11330.27	12605.50	13960.63	15397.09	16916.52
4	6114.03	7006.02	7972.52	9014.71	10133.71	11330.27	12605.50	13960.63	15397.09	16916.52
5	6114.03	7005.23	7975.05	9011.40	10144.66	11323.91	12616.04	14018.66	15422.55	16870.09
6	6114.27	7006.02	7972.52	9014.71	10133.71	11330.27	12605.50	13960.63	15397.09	16916.52
7	6114.27	7006.02	7972.52	9014.71	10133.71	11330.27	12605.50	13960.63	15397.09	16916.71
8	6115.38	7026.93	8002.58	9014.50	10131.20	11326.63	12608.77	14538.75	15411.56	16941.55
9	6114.27	7006.02	7972.52	9014.71	10133.71	11330.27	12605.50	13960.63	15397.09	16916.71
10	6114.27	7006.02	7972.52	9014.71	10133.71	11330.27	12605.50	13960.63	15397.09	16916.71
11	6129.82	7008.02	7976.51	9016.57	10142.61	11328.90	12625.99	13969.64	15400.50	16903.12
12	6114.27	7006.02	7972.52	9014.71	10133.71	11330.27	12605.50	13960.63	15397.09	16916.71
MATPOWER	6114.27	7006.02	7972.52	9014.71	10133.71	11330.27	12605.50	13960.63	15412.54	17004.28

TABLE XII
COMPUTATIONAL TIME OF EXACT OPF MODEL FOR HEAVY POWER LOADS OF CASE9

Format	Computational time (s)									
	110%	120%	130%	140%	150%	160%	170%	180%	190%	200%
1	0.05	0.05	0.05	0.03	0.03	0.03	0.05	0.03	0.08	0.05
2	0.17	0.23	1.06	0.53	0.25	0.08	0.19	0.31	0.08	0.08
3	0.05	0.03	0.03	0.03	0.03	0.03	0.05	0.03	0.08	0.05
4	0.06	0.03	0.05	0.08	0.03	0.03	0.05	0.03	0.19	0.03
5	0.38	0.89	0.09	0.13	1.34	0.09	0.11	0.03	0.44	0.38
6	0.06	0.03	0.05	0.08	0.03	0.03	0.06	0.08	0.06	0.03
7	0.06	0.03	0.05	0.14	0.06	0.03	0.03	0.14	0.06	0.03
8	0.22	3.00	0.66	0.08	0.67	0.05	0.34	0.34	2.09	1.44
9	0.06	0.05	0.05	0.06	0.06	0.05	0.03	0.24	0.05	0.03
10	0.05	0.08	0.06	0.09	0.05	0.03	0.03	0.09	0.08	0.06
11	0.16	0.27	0.47	0.27	0.42	1.45	0.31	0.33	0.88	0.27
12	0.06	0.08	0.08	0.13	0.05	0.03	0.03	0.06	0.08	0.05
MATPOWER	1.03	1.05	1.14	1.30	1.31	1.25	1.28	1.30	1.40	1.25

TABLE XIII
OBJECTIVE SOLUTIONS OF EXACT OPF MODEL FOR HEAVY POWER LOADS OF IEEE118

Format	Objective solution ($)									
	110%	120%	130%	140%	150%	160%	170%	180%	190%	200%
1	146584.41	163717.23	181026.22	198505.38	216185.52	234071.02	252203.09	270661.72	289547.38	309049.00
2	146629.57	163767.22	181076.43	198565.32	216389.18	234301.10	252464.21	270747.87	289855.94	309115.65
3	146584.41	163717.23	181026.22	198505.38	216185.52	234071.02	252203.09	270661.72	289547.37	309049.00
4	146584.34	163717.15	181026.15	198505.31	216185.44	234070.99	252203.09	270661.72	289547.49	309049.23
5	146674.46	163811.03	181123.74	198611.39	216447.91	234459.16	270777.81	271214.68	290280.28	309101.80
6	146584.34	163717.15	181026.15	198505.31	216185.44	234070.99	252203.09	270661.76	289547.49	309049.23
7	146584.41	163717.23	181026.22	198505.38	216185.52	234071.02	252203.09	270661.72	289547.38	309049.00
8	146629.57	163767.22	1810076.43	198565.32	216389.18	234301.10	252464.21	270747.87	289855.94	309115.65
9	146584.41	163717.23	181026.22	198505.38	216185.52	234071.02	252203.09	270661.72	289547.38	309049.00
10	146584.34	163717.15	181026.15	198505.31	216185.52	234070.99	252203.09	270661.76	289547.49	309049.23
11	146674.46	163811.03	181123.74	198611.39	216447.91	234459.16	252629.32	271214.68	290280.28	309101.80
12	146584.34	163717.15	181026.15	198505.31	216185.44	234070.99	252203.09	270661.76	289547.49	309049.23
MATPOWER	146584.49	163717.30	181026.29	198505.42	216185.54	234070.66	252202.15	270659.85	289544.15	309043.83

TABLE XIV
COMPUTATIONAL TIME OF EXACT OPF MODEL FOR HEAVY POWER LOADS OF IEEE118

Format	Computational time (s)									
	110%	120%	130%	140%	150%	160%	170%	180%	190%	200%
1	0.16	0.22	0.19	0.20	0.39	0.25	0.22	0.20	0.23	0.22
2	0.42	0.50	0.47	0.72	0.45	0.47	0.78	0.66	0.61	0.63
3	0.19	0.17	0.17	0.20	0.36	0.28	0.27	0.22	0.22	0.24
4	0.17	0.16	0.20	0.25	0.38	0.30	0.22	0.22	0.22	0.24
5	0.47	0.38	0.50	0.83	0.84	0.50	0.70	0.69	0.97	0.89
6	0.16	0.16	0.19	0.23	0.39	0.23	0.25	0.22	0.22	0.25
7	0.16	0.16	0.16	0.24	0.38	0.25	0.23	0.24	0.22	0.25
8	0.41	0.53	0.45	0.64	0.44	0.48	0.77	0.67	0.58	0.63
9	0.19	0.14	0.16	0.19	0.36	0.28	0.20	0.20	0.20	0.22
10	0.20	0.19	0.20	0.27	0.44	0.31	0.25	0.24	0.25	0.25
11	0.47	0.38	0.48	0.80	0.89	0.49	0.67	0.70	0.98	0.83
12	0.16	0.16	0.16	0.22	0.39	0.23	0.22	0.22	0.22	0.23
MATPOWER	1.77	1.90	1.77	2.09	1.98	1.84	1.89	1.98	1.97	2.14

TABLE XV
OBJECTIVE SOLUTIONS OF APPROXIMATE OPF MODEL FOR HEAVY POWER LOADS OF CASE9

Format	Objective solution ($)									
	110%	120%	130%	140%	150%	160%	170%	180%	190%	200%
1	6114.28	7006.04	7972.55	9014.76	10133.79	11330.38	12605.65	13960.84	15397.39	16916.93
2	6114.14	7005.57	7971.77	9013.35	10131.27	11326.73	12600.42	13953.45	15387.04	16902.57
3	6114.28	7006.04	7972.55	9014.76	10133.79	11330.38	12605.65	13960.84	15397.39	16916.93
4	6113.90	7005.22	7971.39	9013.32	10131.76	11327.56	12601.78	13955.60	15390.36	16907.56
5	6113.81	7004.94	7970.87	9012.09	10129.56	11324.30	12597.02	13948.75	15380.63	16893.90
6	6113.90	7005.22	7971.39	9013.32	10131.76	11327.56	12601.78	13955.60	15390.36	16907.56
7	6114.28	7006.04	7972.55	9014.76	10133.79	11330.38	12605.65	13960.84	15397.39	16917.12
8	6114.14	7005.57	7971.77	9013.35	10131.27	11326.73	12600.42	13953.45	15387.04	16902.57
9	6114.28	7006.04	7972.55	9014.76	10133.79	11330.38	12605.65	13960.84	15397.39	16917.12
10	6113.90	7005.22	7971.39	9013.32	10131.76	11327.56	12601.78	13955.60	15390.36	16907.56
11	6113.81	7004.94	7970.87	9012.09	10129.56	11324.30	12607.02	13948.75	15380.63	16893.90
12	6113.90	7005.22	7971.39	9013.32	10131.76	11327.56	12601.78	13955.60	15390.36	16907.56

TABLE XVI
COMPUTATIONAL TIME OF APPROXIMATE OPF MODEL FOR HEAVY POWER LOADS OF CASE9

Format	Computational time (s)									
	110%	120%	130%	140%	150%	160%	170%	180%	190%	200%
1	0.03	0.05	0.03	0.03	0.03	0.05	0.05	0.03	0.03	0.03
2	0.03	0.05	0.03	0.05	0.05	0.03	0.05	0.03	0.03	0.03
3	0.03	0.03	0.05	0.05	0.05	0.03	0.05	0.06	0.03	0.03
4	0.05	0.05	0.05	0.05	0.03	0.06	0.05	0.03	0.03	0.03
5	0.05	0.05	0.05	0.05	0.05	0.05	0.05	0.03	0.05	0.05
6	0.03	0.05	0.03	0.05	0.03	0.05	0.05	0.06	0.05	0.03
7	0.03	0.05	0.03	0.03	0.03	0.06	0.03	0.05	0.03	0.03
8	0.03	0.05	0.05	0.05	0.05	0.03	0.03	0.03	0.05	0.03
9	0.03	0.03	0.03	0.05	0.03	0.05	0.05	0.06	0.03	0.05
10	0.03	0.03	0.03	0.03	0.03	0.06	0.03	0.03	0.03	0.05
11	0.05	0.03	0.05	0.05	0.05	0.05	0.03	0.03	0.03	0.03
12	0.03	0.03	0.03	0.05	0.03	0.05	0.03	0.03	0.03	0.03

TABLE XVII
THE MAXIMUM APPROXIMATION GAP OF ACTIVE POWER LOSS OF APPROXIMATE OPF MODEL FOR HEAVY POWER LOADS OF CASE9

Format	The maximum approximation gap									
	110%	120%	130%	140%	150%	160%	170%	180%	190%	200%
1	0.00×10^{0}	0.00×10^{0}	0.00×10^{0}	0.00×10^{0}	0.00×10^{0}	0.00×10^{0}	0.00×10^{0}	0.00×10^{0}	0.00×10^{0}	0.00×10^{0}
2	1.87×10^{-15}	2.11×10^{-13}	1.47×10^{-13}	3.57×10^{-13}	5.27×10^{-13}	5.47×10^{-15}	2.43×10^{-13}	1.85×10^{-13}	1.21×10^{-13}	1.69×10^{-13}
3	0.00×10^{0}	0.00×10^{0}	0.00×10^{0}	0.00×10^{0}	0.00×10^{0}	0.00×10^{0}	0.00×10^{0}	0.00×10^{0}	0.00×10^{0}	0.00×10^{0}
4	0.00×10^{0}	0.00×10^{0}	0.00×10^{0}	0.00×10^{0}	0.00×10^{0}	0.00×10^{0}	0.00×10^{0}	0.00×10^{0}	0.00×10^{0}	0.00×10^{0}
5	1.70×10^{-14}	1.88×10^{-13}	6.11×10^{-13}	4.11×10^{-13}	3.33×10^{-13}	2.62×10^{-13}	1.93×10^{-13}	3.14×10^{-15}	1.27×10^{-15}	7.81×10^{-15}
6	0.00×10^{0}	0.00×10^{0}	0.00×10^{0}	0.00×10^{0}	0.00×10^{0}	0.00×10^{0}	0.00×10^{0}	0.00×10^{0}	0.00×10^{0}	0.00×10^{0}
7	0.00×10^{0}	0.00×10^{0}	0.00×10^{0}	0.00×10^{0}	0.00×10^{0}	0.00×10^{0}	0.00×10^{0}	0.00×10^{0}	0.00×10^{0}	0.00×10^{0}
8	7.09×10^{-11}	7.14×10^{-11}	7.19×10^{-11}	7.30×10^{-11}	7.31×10^{-11}	7.39×10^{-11}	7.47×10^{-11}	7.56×10^{-11}	7.65×10^{-11}	7.75×10^{-11}
9	0.00×10^{0}	0.00×10^{0}	0.00×10^{0}	0.00×10^{0}	0.00×10^{0}	0.00×10^{0}	0.00×10^{0}	0.00×10^{0}	0.00×10^{0}	0.00×10^{0}
10	0.00×10^{0}	0.00×10^{0}	0.00×10^{0}	0.00×10^{0}	0.00×10^{0}	0.00×10^{0}	0.00×10^{0}	0.00×10^{0}	0.00×10^{0}	0.00×10^{0}
11	7.09×10^{-11}	7.18×10^{-11}	7.18×10^{-11}	7.23×10^{-11}	7.30×10^{-11}	7.37×10^{-11}	7.45×10^{-11}	7.53×10^{-11}	7.62×10^{-11}	7.71×10^{-11}
12	0.00×10^{0}	0.00×10^{0}	0.00×10^{0}	0.00×10^{0}	0.00×10^{0}	0.00×10^{0}	0.00×10^{0}	0.00×10^{0}	0.00×10^{0}	0.00×10^{0}

TABLE XVIII
THEMAXIMUM APPROXIMATION GAP OF REACTIVE POWER LOSS OF APPROXIMATE OPF MODEL FOR HEAVY POWER LOADS OF CASE9

Format	The maximum approximation gap									
	110%	120%	130%	140%	150%	160%	170%	180%	190%	200%
1	2.54×10^{-1}	1.57×10^{-1}	5.82×10^{-2}	3.28×10^{-10}	1.60×10^{-10}	2.69×10^{-11}	7.64×10^{-11}	1.57×10^{-10}	2.21×10^{-10}	2.72×10^{-10}
2	1.84×10^{-1}	1.21×10^{-1}	4.41×10^{-2}	6.27×10^{-10}	7.08×10^{-10}	6.71×10^{-10}	6.68×10^{-10}	6.70×10^{-10}	6.73×10^{-10}	6.77×10^{-10}
3	2.55×10^{-1}	1.57×10^{-1}	5.84×10^{-2}	1.88×10^{0}	1.82×10^{0}	2.68×10^{-11}	7.65×10^{-11}	1.57×10^{-10}	2.21×10^{-10}	2.72×10^{-10}
4	2.04×10^{0}	2.00×10^{0}	1.95×10^{0}	1.50×10^{0}	1.81×10^{0}	1.74×10^{0}	1.66×10^{0}	1.58×10^{0}	1.50×10^{0}	1.41×10^{0}
5	1.65×10^{0}	1.60×10^{0}	1.54×10^{0}	1.88×10^{0}	1.44×10^{0}	1.37×10^{0}	1.29×10^{0}	1.22×10^{0}	1.14×10^{0}	1.06×10^{0}
6	1.99×10^{0}	2.00×10^{0}	1.95×10^{0}	3.29×10^{-10}	1.82×10^{0}	1.74×10^{0}	1.67×10^{0}	1.58×10^{0}	1.49×10^{0}	1.41×10^{0}
7	2.04×10^{-1}	1.40×10^{-1}	5.56×10^{-2}	3.29×10^{-10}	1.60×10^{-10}	2.72×10^{-11}	7.62×10^{-11}	1.57×10^{-10}	2.21×10^{-10}	2.90×10^{-10}
8	1.16×10^{-1}	8.08×10^{-2}	2.90×10^{-2}	6.18×10^{-10}	6.95×10^{-10}	6.67×10^{-10}	6.33×10^{-10}	6.65×10^{-10}	6.68×10^{-10}	6.72×10^{-10}
9	2.04×10^{-1}	1.39×10^{-1}	5.50×10^{-2}	3.30×10^{-10}	1.60×10^{-10}	2.71×10^{-11}	7.62×10^{-11}	1.57×10^{-10}	2.21×10^{-10}	2.89×10^{-10}
10	1.71×10^{-1}	1.56×10^{-1}	1.40×10^{-1}	1.22×10^{-1}	1.04×10^{-1}	8.41×10^{-2}	6.41×10^{-2}	4.33×10^{-2}	2.19×10^{-2}	2.06×10^{-10}
11	8.28×10^{-2}	6.24×10^{-2}	3.95×10^{-2}	1.44×10^{-2}	6.75×10^{-10}	6.62×10^{-10}	6.31×10^{-10}	6.62×10^{-10}	6.64×10^{-10}	6.68×10^{-10}
12	1.71×10^{-1}	1.56×10^{-1}	1.40×10^{-1}	1.22×10^{-1}	1.04×10^{-1}	8.43×10^{-2}	6.48×10^{-2}	4.26×10^{-2}	2.18×10^{-2}	2.08×10^{-10}

TABLE XIX
OBJECTIVE SOLUTION OF APPROXIMATE OPF MODEL FOR HEAVY POWER LOADS OF IEEE118

Format	Objective solution ($)									
	110%	120%	130%	140%	150%	160%	170%	180%	190%	200%
1	146544.37	163678.09	180986.97	198463.56	216139.58	234018.65	252135.44	270575.68	289444.00	308925.65
2	146550.23	163683.12	180991.60	198467.97	216143.89	234022.81	252138.26	270569.30	289423.11	308888.97
3	146551.11	163684.06	180992.61	198469.05	216145.06	234024.47	252141.43	270580.54	289448.93	308931.22
4	146531.65	163664.05	180971.26	198444.66	216115.93	233989.29	252097.65	270522.21	289373.44	308833.42
5	146538.89	163671.16	180978.35	198451.76	216123.05	233996.20	252103.35	270522.29	289357.32	308797.67
6	146540.11	163672.48	180979.76	198453.28	216124.68	233998.00	252107.05	270533.23	289384.36	308843.26
7	146544.37	163678.09	180986.97	198463.56	216139.58	234018.65	252135.44	270575.68	289444.00	308925.65
8	146550.23	163683.12	180991.60	198467.97	216143.89	234022.81	252138.26	270569.30	289423.11	308888.97
9	146551.11	163684.06	180992.61	198469.05	216145.06	234024.47	252141.43	270580.54	289448.93	308931.22
10	146531.65	163664.05	180971.26	198444.66	216115.93	233989.29	252097.65	270522.21	289373.44	308833.42
11	146538.89	163671.16	180978.35	198451.76	216123.05	233996.20	252103.35	270522.29	289357.32	308797.67
12	146540.11	163672.48	180979.76	198453.28	216124.68	233998.00	252107.05	270533.23	289384.36	308843.26

TABLE XX
COMPUTATIONAL TIME OF APPROXIMATE OPF MODEL FOR HEAVY POWER LOADS OF IEEE118

Format	Computational time (s)									
	110%	120%	130%	140%	150%	160%	170%	180%	190%	200%
1	0.53	0.80	0.66	0.52	0.50	0.52	0.52	0.50	0.50	0.64
2	0.91	0.88	1.00	0.78	0.92	0.78	0.76	0.78	0.95	0.86
3	0.66	0.42	0.56	0.33	0.36	0.41	0.34	0.36	0.36	0.41
4	0.44	0.52	0.53	0.45	0.44	0.42	0.44	0.45	0.58	0.55
5	1.00	0.81	0.84	0.86	0.92	0.98	0.80	0.83	0.72	0.84
6	0.39	0.44	0.45	0.34	0.36	0.38	0.36	0.41	0.41	0.45
7	0.50	0.83	0.64	0.50	0.50	0.50	0.50	0.50	0.50	0.62
8	0.89	0.91	1.01	0.78	0.97	0.77	0.81	0.75	0.97	0.81
9	0.67	0.45	0.56	0.36	0.39	0.36	0.34	0.36	0.36	0.39
10	0.45	0.58	0.50	0.47	0.52	0.44	0.44	0.45	0.52	0.56
11	0.97	0.84	0.78	0.88	0.94	0.95	0.80	0.78	0.77	0.84
12	0.39	0.44	0.42	0.36	0.36	0.36	0.36	0.41	0.39	0.48

TABLE XXI
THE MAXIMUM APPROXIMATION GAP OF ACTIVE POWER LOSS OF APPROXIMATE OPF MODEL FOR HEAVY POWER LOADS OF IEEE118

Format	The maximum approximation gap									
	110%	120%	130%	140%	150%	160%	170%	180%	190%	200%
1	0.00×10^{0}	0.00×10^{0}	0.00×10^{0}	0.00×10^{0}	0.00×10^{0}	0.00×10^{0}	0.00×10^{0}	0.00×10^{0}	0.00×10^{0}	0.00×10^{0}
2	2.56×10^{-10}	2.57×10^{-12}	2.58×10^{-12}	2.58×10^{-12}	2.58×10^{-12}	2.58×10^{-12}	2.57×10^{-12}	2.57×10^{-12}	2.56×10^{-12}	2.57×10^{-12}
3	0.00×10^{0}	0.00×10^{0}	0.00×10^{0}	0.00×10^{0}	0.00×10^{0}	0.00×10^{0}	0.00×10^{0}	0.00×10^{0}	0.00×10^{0}	0.00×10^{0}
4	0.00×10^{0}	0.00×10^{0}	0.00×10^{0}	0.00×10^{0}	0.00×10^{0}	0.00×10^{0}	0.00×10^{0}	0.00×10^{0}	0.00×10^{0}	0.00×10^{0}
5	2.95×10^{-12}	2.55×10^{-12}	2.56×10^{-12}	2.56×10^{-12}	2.57×10^{-12}	2.57×10^{-12}	2.58×10^{-12}	2.57×10^{-12}	2.54×10^{-12}	2.54×10^{-12}
6	0.00×10^{0}	0.00×10^{0}	0.00×10^{0}	0.00×10^{0}	0.00×10^{0}	0.00×10^{0}	0.00×10^{0}	0.00×10^{0}	0.00×10^{0}	0.00×10^{0}
7	0.00×10^{0}	0.00×10^{0}	0.00×10^{0}	0.00×10^{0}	0.00×10^{0}	0.00×10^{0}	0.00×10^{0}	0.00×10^{0}	0.00×10^{0}	0.00×10^{0}
8	2.56×10^{-12}	2.57×10^{-12}	2.58×10^{-12}	2.58×10^{-12}	2.58×10^{-12}	2.58×10^{-12}	2.57×10^{-12}	2.57×10^{-12}	2.56×10^{-12}	2.57×10^{-12}
9	0.00×10^{0}	0.00×10^{0}	0.00×10^{0}	0.00×10^{0}	0.00×10^{0}	0.00×10^{0}	0.00×10^{0}	0.00×10^{0}	0.00×10^{0}	0.00×10^{0}
10	0.00×10^{0}	0.00×10^{0}	0.00×10^{0}	0.00×10^{0}	0.00×10^{0}	0.00×10^{0}	0.00×10^{0}	0.00×10^{0}	0.00×10^{0}	0.00×10^{0}
11	2.95×10^{-12}	2.55×10^{-12}	2.56×10^{-12}	2.56×10^{-12}	2.57×10^{-12}	2.57×10^{-12}	2.58×10^{-12}	2.57×10^{-12}	2.54×10^{-12}	2.54×10^{-12}
12	0.00×10^{0}	0.00×10^{0}	0.00×10^{0}	0.00×10^{0}	0.00×10^{0}	0.00×10^{0}	0.00×10^{0}	0.00×10^{0}	0.00×10^{0}	0.00×10^{0}

TABLE XXII
THE MAXIMUM APPROXIMATION GAP OF REACTIVE POWER LOSS OF APPROXIMATE OPF MODEL FOR HEAVY POWER LOADS OF IEEE118

Format	The maximum approximation gap ($\times 10^0$)									
	110%	120%	130%	140%	150%	160%	170%	180%	190%	200%
1	6.07	6.09	6.09	6.05	5.98	5.73	5.56	5.00	4.59	4.08
2	3.99	4.00	4.02	4.03	4.05	4.03	4.03	4.01	3.97	3.92
3	4.24	4.25	4.25	7.40	2.29	4.28	4.28	4.26	4.21	4.16
4	7.42	7.42	7.41	2.76	7.39	7.39	7.38	7.38	7.38	7.37
5	2.92	2.88	2.82	2.76	2.69	2.63	2.54	2.50	2.69	2.66
6	3.42	3.37	3.32	3.26	3.19	3.13	3.05	3.12	3.01	2.88
7	6.07	6.09	6.09	6.05	5.99	5.73	5.55	5.00	4.59	4.08
8	3.99	4.00	4.02	4.03	4.05	4.04	4.03	4.01	3.97	3.92
9	4.24	4.25	4.26	4.28	4.29	4.28	4.28	4.26	4.21	4.16
10	7.42	7.42	7.41	7.40	7.39	7.39	7.38	7.38	7.38	7.37
11	2.92	2.88	2.82	2.76	2.69	2.63	2.54	2.50	2.69	2.66
12	3.42	3.37	3.32	3.26	3.19	3.13	3.05	3.12	3.01	2.88

IV. APPROXIMATION GAP REDUCTION

To reduce the approximation gap of the reactive power loss for the approximate OPF model, a penalty function based method which adds an penalty term $\xi \sum_l q_{ol}$ to the original objective function of the OPF model is proposed as:

$$f' = f(p_n) + \xi \sum_l q_{o_l} \tag{46}$$

where the penalty coefficient $\xi > 0$. In this paper, $\xi = 0.3$ is used.

A. Base Power Loads

The performance of the proposed penalty function based approximation gap reduction method to tighten the approximation gap in the base power loads is shown in Tables XXIII and XXIV. It can be observed that the approximation gaps of the reactive power loss are much smaller than the values listed in Table X. For the maximum approximation gaps of the active power loss, the values are more or less the same compared with the results listed in Table IX. Since the maximum approximation gaps of the active power loss are very small, it is not necessary to reduce them.

B. Heavy Power Loads

The performance of the proposed penalty function based approximation gap reduction method to tighten the approximation gap in the heavy power loads for case9 is shown in Tables XXV and XXVI. The performance of the proposed method to tighten the approximation gap in the heavy power loads for IEEE118 is shown in Tables XXVII and XXVIII. It can be observed that the approximation gaps of the reactive power loss are much smaller than the values listed in Tables XVIII and XVII. These results show that the proposed method is also useful for the power networks in heavy power loads.

TABLE XXIII
REDUCED MAXIMUM APPROXIMATION GAP OF ACTIVE POWER LOSS OF APPROXIMATE OPF MODEL FOR BASE POWER LOADS

Format	Reduced maximum approximation gap								
	case9	IEEE14	case30	IEEE57	case89pegase	IEEE118	ACTIVSg200	IEEE300	ACTIVSg500
1	0.00×10^{0}	0.00×10^{0}	0.00×10^{0}	0.00×10^{0}	9.41×10^{-10}	0.00×10^{0}	1.96×10^{-12}	3.70×10^{-7}	7.21×10^{-14}
2	3.68×10^{-15}	1.29×10^{-10}	6.60×10^{-15}	8.12×10^{-11}	2.83×10^{-9}	2.72×10^{-12}	7.77×10^{-13}	3.99×10^{-8}	5.71×10^{-13}
3	0.00×10^{0}	0.00×10^{0}	0.00×10^{0}	0.00×10^{0}	6.12×10^{-12}	0.00×10^{0}	7.77×10^{-13}	7.34×10^{-8}	5.71×10^{-13}
4	0.00×10^{0}	0.00×10^{0}	0.00×10^{0}	0.00×10^{0}	3.11×10^{-8}	0.00×10^{0}	1.96×10^{-12}	4.55×10^{-7}	7.17×10^{-14}
5	1.09×10^{-14}	1.30×10^{-10}	3.55×10^{-15}	7.19×10^{-11}	2.44×10^{-11}	2.72×10^{-12}	1.37×10^{-12}	6.97×10^{-8}	5.66×10^{-13}
6	0.00×10^{0}	0.00×10^{0}	0.00×10^{0}	0.00×10^{0}	6.15×10^{-12}	0.00×10^{0}	7.80×10^{-13}	1.61×10^{-3}	5.66×10^{-13}
7	0.00×10^{0}	0.00×10^{0}	0.00×10^{0}	0.00×10^{0}	3.11×10^{-8}	0.00×10^{0}	1.96×10^{-12}	3.70×10^{-7}	7.21×10^{-14}
8	7.08×10^{-11}	1.29×10^{-10}	1.04×10^{-9}	8.13×10^{-11}	1.16×10^{-7}	2.72×10^{-12}	1.37×10^{-12}	3.99×10^{-8}	5.71×10^{-13}
9	0.00×10^{0}	0.00×10^{0}	0.00×10^{0}	0.00×10^{0}	6.12×10^{-12}	0.00×10^{0}	7.77×10^{-13}	7.34×10^{-8}	5.71×10^{-13}
10	0.00×10^{0}	0.00×10^{0}	0.00×10^{0}	0.00×10^{0}	1.24×10^{-11}	0.00×10^{0}	1.96×10^{-12}	4.55×10^{-7}	7.17×10^{-14}
11	7.07×10^{-11}	1.30×10^{-10}	2.84×10^{-9}	7.19×10^{-11}	2.44×10^{-11}	2.72×10^{-12}	7.80×10^{-13}	6.97×10^{-8}	5.66×10^{-13}
12	0.00×10^{0}	0.00×10^{0}	0.00×10^{0}	0.00×10^{0}	6.15×10^{-12}	0.00×10^{0}	7.80×10^{-13}	1.61×10^{-3}	5.66×10^{-13}

TABLE XXIV
REDUCED MAXIMUM APPROXIMATION GAP OF REACTIVE POWER LOSS OF APPROXIMATE OPF MODEL FOR BASE POWER LOADS

Format	Reduced maximum approximation gap								
	case9	IEEE14	case30	IEEE57	case89pegase	IEEE118	ACTIVSg200	IEEE300	ACTIVSg500
1	3.94×10^{-10}	3.62×10^{-10}	1.04×10^{-10}	7.21×10^{-11}	8.50×10^{-11}	4.38×10^{-11}	7.05×10^{-11}	4.75×10^{-2}	1.95×10^{-10}
2	6.64×10^{-10}	4.74×10^{-10}	1.76×10^{-10}	8.00×10^{-12}	4.56×10^{-8}	3.43×10^{-10}	9.84×10^{-12}	3.09×10^{-2}	9.38×10^{-12}
3	3.95×10^{-10}	4.07×10^{-10}	1.76×10^{-10}	8.94×10^{-11}	9.61×10^{-11}	3.25×10^{-11}	9.84×10^{-12}	7.53×10^{-7}	9.38×10^{-12}
4	3.94×10^{-10}	3.56×10^{-10}	1.05×10^{-10}	3.09×10^{-2}	1.86×10^{-7}	4.39×10^{-11}	7.06×10^{-11}	8.96×10^{-2}	1.84×10^{-10}
5	5.74×10^{-10}	4.42×10^{-10}	1.77×10^{-10}	5.00×10^{-2}	2.10×10^{-9}	2.02×10^{-9}	2.07×10^{-11}	3.04×10^{-2}	9.44×10^{-12}
6	3.94×10^{-10}	4.11×10^{-10}	1.77×10^{-10}	3.09×10^{-2}	9.58×10^{-11}	3.24×10^{-11}	9.87×10^{-12}	4.60×10^{-2}	9.44×10^{-12}
7	3.94×10^{-10}	3.62×10^{-10}	1.04×10^{-10}	7.21×10^{-11}	1.13×10^{-7}	4.38×10^{-11}	7.05×10^{-11}	4.75×10^{-2}	1.95×10^{-10}
8	6.60×10^{-10}	4.74×10^{-10}	4.03×10^{-9}	8.00×10^{-12}	8.36×10^{-7}	3.43×10^{-10}	2.07×10^{-11}	3.09×10^{-2}	9.38×10^{-12}
9	3.95×10^{-10}	4.07×10^{-10}	1.76×10^{-10}	8.94×10^{-11}	9.61×10^{-11}	3.25×10^{-11}	9.84×10^{-12}	7.53×10^{-7}	9.38×10^{-12}
10	3.94×10^{-10}	3.56×10^{-10}	1.05×10^{-10}	3.09×10^{-2}	3.31×10^{-11}	4.39×10^{-11}	7.06×10^{-11}	8.96×10^{-2}	1.84×10^{-10}
11	5.72×10^{-10}	4.42×10^{-10}	1.14×10^{-8}	5.00×10^{-2}	2.10×10^{-9}	2.02×10^{-9}	9.87×10^{-12}	3.04×10^{-2}	9.44×10^{-12}
12	3.94×10^{-10}	4.11×10^{-10}	1.77×10^{-10}	3.09×10^{-2}	9.62×10^{-11}	3.24×10^{-11}	9.87×10^{-12}	4.60×10^{-2}	9.44×10^{-12}

TABLE XXV
REDUCED MAXIMUM APPROXIMATION GAP OF ACTIVE POWER LOSS OF APPROXIMATE OPF MODEL FOR HEAVY POWER LOADS OF CASE9

Format	Reduced maximum approximation gap									
	110%	120%	130%	140%	150%	160%	170%	180%	190%	200%
1	0.00×10^{0}	0.00×10^{0}	0.00×10^{0}	0.00×10^{0}	0.00×10^{0}	0.00×10^{0}	0.00×10^{0}	0.00×10^{0}	0.00×10^{0}	0.00×10^{0}
2	4.18×10^{-14}	8.69×10^{-14}	7.43×10^{-15}	6.67×10^{-14}	2.96×10^{-13}	1.21×10^{-13}	3.65×10^{-13}	1.59×10^{-14}	1.05×10^{-13}	1.48×10^{-13}
3	0.00×10^{0}	0.00×10^{0}	0.00×10^{0}	0.00×10^{0}	0.00×10^{0}	0.00×10^{0}	0.00×10^{0}	0.00×10^{0}	0.00×10^{0}	0.00×10^{0}
4	0.00×10^{0}	0.00×10^{0}	0.00×10^{0}	0.00×10^{0}	0.00×10^{0}	0.00×10^{0}	0.00×10^{0}	0.00×10^{0}	0.00×10^{0}	0.00×10^{0}
5	3.84×10^{-14}	5.19×10^{-14}	4.69×10^{-14}	1.84×10^{-14}	4.65×10^{-14}	1.69×10^{-14}	8.38×10^{-14}	1.57×10^{-13}	1.56×10^{-13}	8.63×10^{-15}
6	0.00×10^{0}	0.00×10^{0}	0.00×10^{0}	0.00×10^{0}	0.00×10^{0}	0.00×10^{0}	0.00×10^{0}	0.00×10^{0}	0.00×10^{0}	0.00×10^{0}
7	0.00×10^{0}	0.00×10^{0}	0.00×10^{0}	0.00×10^{0}	0.00×10^{0}	0.00×10^{0}	0.00×10^{0}	0.00×10^{0}	0.00×10^{0}	0.00×10^{0}
8	7.11×10^{-11}	7.14×10^{-11}	7.20×10^{-11}	7.25×10^{-11}	7.32×10^{-11}	7.40×10^{-11}	7.48×10^{-11}	7.56×10^{-11}	7.65×10^{-11}	7.75×10^{-11}
9	0.00×10^{0}	0.00×10^{0}	0.00×10^{0}	0.00×10^{0}	0.00×10^{0}	0.00×10^{0}	0.00×10^{0}	0.00×10^{0}	0.00×10^{0}	0.00×10^{0}
10	0.00×10^{0}	0.00×10^{0}	0.00×10^{0}	0.00×10^{0}	0.00×10^{0}	0.00×10^{0}	0.00×10^{0}	0.00×10^{0}	0.00×10^{0}	0.00×10^{0}
11	7.10×10^{-11}	7.19×10^{-11}	7.19×10^{-11}	7.24×10^{-11}	7.30×10^{-11}	7.38×10^{-11}	7.45×10^{-11}	7.54×10^{-11}	7.65×10^{-11}	7.71×10^{-11}
12	0.00×10^{0}	0.00×10^{0}	0.00×10^{0}	0.00×10^{0}	0.00×10^{0}	0.00×10^{0}	0.00×10^{0}	0.00×10^{0}	0.00×10^{0}	0.00×10^{0}

TABLE XXVI
REDUCED MAXIMUM APPROXIMATION GAP OF REACTIVE POWER LOSS OF APPROXIMATE OPF MODEL FOR HEAVY POWER LOADS OF CASE9

Format	Reduced maximum approximation gap ($\times10^{-10}$)									
	110%	120%	130%	140%	150%	160%	170%	180%	190%	200%
1	3.97	4.00	4.03	4.09	4.12	4.15	4.17	4.21	4.24	4.28
2	6.03	7.06	6.66	6.48	6.99	6.71	6.69	6.70	6.73	6.78
3	3.97	4.00	4.03	4.09	4.12	4.14	4.17	4.21	4.24	4.28
4	3.99	4.04	4.01	4.16	4.19	4.22	4.26	4.30	4.34	4.38
5	6.03	8.26	6.78	6.54	6.23	6.66	6.65	6.66	6.70	6.56
6	3.99	4.04	4.01	4.16	4.19	4.22	4.26	4.30	4.34	4.38
7	3.97	4.00	4.03	4.09	4.12	4.15	4.17	4.21	4.24	4.29
8	6.21	6.05	6.62	6.43	6.99	6.67	6.64	6.66	6.69	6.73
9	3.97	4.00	4.03	4.09	4.12	4.15	4.17	4.21	4.24	4.29
10	3.99	4.04	4.01	4.16	4.19	4.22	4.26	4.30	4.34	4.38
11	6.28	8.26	6.74	6.50	6.76	6.61	6.60	6.62	6.48	6.69
12	3.99	4.04	4.01	4.16	4.19	4.22	4.26	4.30	4.34	4.38

TABLE XXVII
REDUCED MAXIMUM APPROXIMATION GAP OF ACTIVE POWER LOSS OF APPROXIMATE OPF MODEL FOR HEAVY POWER LOADS OF IEEE118

Format	Reduced maximum approximation gap									
	110%	120%	130%	140%	150%	160%	170%	180%	190%	200%
1	0.00×10^{0}	0.00×10^{0}	0.00×10^{0}	0.00×10^{0}	0.00×10^{0}	0.00×10^{0}	0.00×10^{0}	0.00×10^{0}	0.00×10^{0}	0.00×10^{0}
2	2.73×10^{-12}	2.73×10^{-12}	2.73×10^{-12}	2.74×10^{-12}	2.75×10^{-12}	2.76×10^{-12}	3.12×10^{-12}	2.78×10^{-12}	2.80×10^{-12}	2.80×10^{-12}
3	0.00×10^{0}	0.00×10^{0}	0.00×10^{0}	0.00×10^{0}	0.00×10^{0}	0.00×10^{0}	0.00×10^{0}	0.00×10^{0}	0.00×10^{0}	0.00×10^{0}
4	0.00×10^{0}	0.00×10^{0}	0.00×10^{0}	0.00×10^{0}	0.00×10^{0}	0.00×10^{0}	0.00×10^{0}	0.00×10^{0}	0.00×10^{0}	0.00×10^{0}
5	2.72×10^{-12}	1.85×10^{-11}	2.73×10^{-12}	2.74×10^{-12}	2.75×10^{-12}	2.76×10^{-12}	2.76×10^{-12}	2.75×10^{-12}	2.74×10^{-12}	2.71×10^{-12}
6	0.00×10^{0}	0.00×10^{0}	0.00×10^{0}	0.00×10^{0}	0.00×10^{0}	0.00×10^{0}	0.00×10^{0}	0.00×10^{0}	0.00×10^{0}	0.00×10^{0}
7	0.00×10^{0}	0.00×10^{0}	0.00×10^{0}	0.00×10^{0}	0.00×10^{0}	0.00×10^{0}	0.00×10^{0}	0.00×10^{0}	0.00×10^{0}	0.00×10^{0}
8	2.73×10^{-12}	2.73×10^{-12}	2.73×10^{-12}	2.74×10^{-12}	2.75×10^{-12}	2.76×10^{-12}	3.12×10^{-12}	2.78×10^{-12}	2.80×10^{-12}	2.80×10^{-12}
9	0.00×10^{0}	0.00×10^{0}	0.00×10^{0}	0.00×10^{0}	0.00×10^{0}	0.00×10^{0}	0.00×10^{0}	0.00×10^{0}	0.00×10^{0}	0.00×10^{0}
10	0.00×10^{0}	0.00×10^{0}	0.00×10^{0}	0.00×10^{0}	0.00×10^{0}	0.00×10^{0}	0.00×10^{0}	0.00×10^{0}	0.00×10^{0}	0.00×10^{0}
11	2.72×10^{-12}	1.85×10^{-11}	2.73×10^{-12}	2.74×10^{-12}	2.75×10^{-12}	2.76×10^{-12}	2.76×10^{-12}	2.75×10^{-12}	2.74×10^{-12}	2.71×10^{-12}
12	0.00×10^{0}	0.00×10^{0}	0.00×10^{0}	0.00×10^{0}	0.00×10^{0}	0.00×10^{0}	0.00×10^{0}	0.00×10^{0}	0.00×10^{0}	0.00×10^{0}

TABLE XXVIII
REDUCED MAXIMUM APPROXIMATION GAP OF REACTIVE POWER LOSS OF APPROXIMATE OPF MODEL FOR HEAVY POWER LOADS OF IEEE118

Format	Reduced maximum approximation gap									
	110%	120%	130%	140%	150%	160%	170%	180%	190%	200%
1	4.39×10^{-11}	4.39×10^{-11}	4.39×10^{-11}	4.39×10^{-11}	4.39×10^{-11}	4.39×10^{-11}	4.39×10^{-11}	4.39×10^{-11}	1.47×10^{-10}	3.11×10^{-10}
2	3.25×10^{-11}	3.25×10^{-11}	1.04×10^{-8}	1.11×10^{-9}	6.88×10^{-9}	4.66×10^{-8}	3.72×10^{-11}	1.05×10^{-7}	3.64×10^{-8}	5.65×10^{-2}
3	3.71×10^{-11}	3.71×10^{-11}	3.27×10^{-11}	3.28×10^{-11}	3.29×10^{-11}	3.30×10^{-11}	3.30×10^{-11}	3.32×10^{-11}	1.48×10^{-10}	2.96×10^{-10}
4	4.40×10^{-11}	4.40×10^{-11}	4.40×10^{-11}	4.40×10^{-11}	4.40×10^{-11}	4.40×10^{-11}	1.47×10^{-10}	5.10×10^{-9}	2.52×10^{-1}	5.25×10^{-1}
5	3.24×10^{-11}	1.65×10^{-11}	3.25×10^{-11}	5.17×10^{-9}	3.27×10^{-11}	1.38×10^{-11}	5.42×10^{-9}	3.28×10^{-11}	3.37×10^{-1}	1.02×10^{0}
6	3.70×10^{-11}	3.25×10^{-11}	3.26×10^{-11}	3.27×10^{-11}	3.27×10^{-11}	3.28×10^{-11}	1.42×10^{-10}	5.10×10^{-9}	4.61×10^{-1}	1.01×10^{0}
7	4.39×10^{-11}	4.39×10^{-11}	4.39×10^{-11}	4.39×10^{-11}	4.39×10^{-11}	4.39×10^{-11}	4.39×10^{-11}	4.39×10^{-11}	1.47×10^{-10}	3.11×10^{-10}
8	4.25×10^{-11}	3.25×10^{-11}	1.04×10^{-8}	1.11×10^{-9}	6.88×10^{-9}	4.66×10^{-8}	3.72×10^{-11}	1.05×10^{-7}	3.64×10^{-8}	5.65×10^{-2}
9	3.71×10^{-11}	3.71×10^{-11}	3.27×10^{-11}	3.28×10^{-11}	3.29×10^{-11}	3.30×10^{-11}	3.30×10^{-11}	3.32×10^{-11}	1.48×10^{-10}	2.96×10^{-10}
10	4.40×10^{-11}	4.40×10^{-11}	4.40×10^{-11}	4.40×10^{-11}	4.40×10^{-11}	4.40×10^{-11}	1.47×10^{-10}	5.10×10^{-9}	2.52×10^{-1}	5.25×10^{-1}
11	3.24×10^{-11}	1.65×10^{-11}	3.25×10^{-11}	5.17×10^{-9}	3.27×10^{-11}	1.38×10^{-11}	5.42×10^{-9}	3.28×10^{-11}	3.37×10^{-1}	1.02×10^{0}
12	3.70×10^{-11}	3.25×10^{-11}	3.26×10^{-11}	3.27×10^{-11}	3.27×10^{-11}	3.28×10^{-11}	1.42×10^{-10}	4.10×10^{-9}	4.61×10^{-1}	1.01×10^{0}

V. CONCLUSION

This paper formulates six formats of the exact General-BranchFlow model and six formats of the approximate General-BranchFlow model. All the formats are valid for both radial and mesh power networks. By taking into account the shunt conductive components of the transmission line Π-model, a linear amapacity constraint is derived. Based on the formulated General-BranchFlow model and the ampacity constraint, twelve formats of the exact OPF model and twelve formats of the approximate OPF model are proposed. Providing different formats of the OPF models gives the power system operators more options in solving the network operation problems when using one format may face numerical difficulties or parameter non-availability problems. The reason of proposing the approximate OPF model is to give a convex formulation which advantages in finding the globally optimal solution using available optimization solvers.

The numerical investigations using various IEEE test cases for different power loads prove the accuracy and computational efficiency of all the twelve formats of the exact and approximate OPF models. For the twelve formats of the approximate OPF model, non-negligible reactive power loss approximation gaps exist for some test cases if the IPOPT solver is used. To reduce the approximation gaps, this paper proposes to use the penalty function in the objective function of the OPF model. The numerical results show that the approximation gaps of reactive power loss are largely reduced. In this way, the AC-feasibility of the approximate General-BranchFlow model is enhanced.

REFERENCES

[1] H. Saadat, *Power System Analysis*. Princeton: McGraw Hill Education, 2004.
[2] J. Carpentier, "Contribution to the economic dispatch problem," *Bulletin de la Societe Francaise des Electriciens*, vol. 3, no. 8, pp. 431-447, Jan. 1962.
[3] J. Carpentier, "Optimal power flows," *International Journal of Electrical Power & Energy Systems*, vol. 1, no. 1, pp. 3-15, Apr. 1979.
[4] R. R. Shoults and D. T. Sun, "Optimal power flow based upon *p-q* decomposition," *IEEE Transactions on Power Apparatus and Systems*, vol. PAS-101, no. 2, pp. 397-405, Feb. 1982.
[5] F. Capitanescu, "Critical review of recent advances and further developments needed in AC optimal power flow," *Electric Power Systems*

Research, vol. 136, pp. 57-68, Jul. 2016.
[6] X. Li, F. Li, H. Yuan *et al.*, "GPU-based fast decoupled power flow with preconditioned iterative solver and inexact Newton method," *IEEE Transactions on Power Systems*, vol. 32, no. 4, pp. 2695-2703, Jul. 2017.
[7] M. B. Cain, R. P. O'neill, A. Castillo *et al.*, "History of optimal power flow and formulations," *Federal Energy Regulatory Commission*, vol. 1, pp. 1-36, Jan. 2012.
[8] P. Chen, X. Xiao, and X. Wang, "Interval optimal power flow applied to distribution networks under uncertainty of loads and renewable resources," *Journal of Modern Power Systems and Clean Energy*, vol. 7, no. 1, pp. 139-150, Jan. 2019.
[9] A. Nawaz and H. Wang, "Risk-aware distributed optimal power flow in coordinated transmission and distribution system," *Journal of Modern Power Systems and Clean Energy*, vol. 9, no. 3, pp. 502-515, May 2021.
[10] J. A. Taylor, "Conic optimization of electric power systems," Ph. D. dissertation, Massachusetts Institute of Technology, Cambridge, USA, 2011.
[11] X. Bai, H. Wei, K. Fujisawa *et al.*, "Semidefinite programming for optimal power flow problems," *International Journal of Electrical Power & Energy Systems*, vol. 30, no. 6, pp. 383-392, Sept. 2008.
[12] B. Ghaddar, J. Marecek, and M. Mevissen, "Optimal power flow as a polynomial optimization problem," *IEEE Transactions on Power Systems*, vol. 31, no. 1, pp. 539-546, Jan. 2016.
[13] S. Huang, Q. Wu, J. Wang *et al*., "A sufficient condition on convex relaxation of ac optimal power flow in distribution networks," *IEEE Transactions on Power Systems*, vol. 32, no. 2, pp. 1359-1368, Mar. 2017.
[14] D. K. Molzahn, J. T. Holzer, B. C. Lesieutre *et al.*, "Implementation of a large-scale optimal power flow solver based on semidefinite programming," *IEEE Transactions on Power Systems*, vol. 28, no. 4, pp. 3987-3998, Nov. 2013.
[15] D. K. Molzahn and I. A. Hiskens, "Sparsity-exploiting moment-based relaxations of the optimal power flow problem," *IEEE Transactions on Power Systems*, vol. 30, no. 6, pp. 3168-3180, Nov. 2015.
[16] M. Baran and F. Wu, "Optimal sizing of capacitors placed on a radial distribution system," *IEEE Transactions on Power Delivery*, vol. 4, no. 1, pp. 735-743, Jan. 1989.
[17] M. Farivar and S. H. Low, "Branch flow model: relaxations and convexification – part I," *IEEE Transactions on Power Systems*, vol. 28, no. 3, pp. 2554-2564, Aug. 2013.
[18] M. Farivar and S. H. Low, "Branch flow model: relaxations and convexification – part II," *IEEE Transactions on Power Systems*, vol. 28, no. 3, pp. 2565-2572, Aug. 2013.
[19] C. Wang, W. Wei, J. Wang *et al.*, "Convex optimization based distributed optimal gas-power flow calculation," *IEEE Transactions on Sustainable Energy*, vol. 9, no. 3, pp. 1145-1156, Jul. 2018.
[20] F. Geth, S. Claeys, and G. Deconinck, "Nonconvex lifted unbalanced branch flow model: derivation, implementation and experiments," *Electric Power Systems Research*, vol. 189, p. 106558, Dec. 2020.
[21] K. Christakou, D.-C. Tomozeic, J.-Y. L. Boudec *et al.*, "AC OPF in radial distribution networks – part I: on the limits of the branch flow convexification and the alternating direction method of multipliers," *Electric Power Systems Research*, vol. 143, pp. 438-450, Feb. 2017.
[22] K. Christakou, D.-C. Tomozeic, J.-Y. L. Boudec *et al.*, "AC OPF in radial distribution networks – part II: an augmented Lagrangian-based OPF algorithm, distributable via primal decomposition," *Electric Power Systems Research*, vol. 150, pp. 24-35, Sept. 2017.
[23] M. Nick, R. Cherkaoui, J.-Y. L. Boudec *et al.*, "An exact convex formulation of the optimal power flow in radial distribution networks including transverse components," *IEEE Transactions on Automatic Control*, vol. 63, no. 3, pp. 682-697, Mar. 2018.
[24] M. Baradar and M. R. Hesamzadeh, "AC power flow representation in conic format," *IEEE Transactions on Power Systems*, vol. 30, no. 1, pp. 546-547, Jan. 2015.
[25] Z. Yuan and M. R. Hesamzadeh, "Second-order cone AC optimal power flow: convex relaxations and feasible solutions," *Journal of Modern Power Systems and Clean Energy*, vol. 7, no. 2, pp. 268-280, Mar. 2019.
[26] Z. Yuan, M. R. Hesamzadeh, and D. Biggar, "Distribution locational marginal pricing by convexified ACOPF and hierarchical dispatch," *IEEE Transactions on Smart Grid*, vol. 9, no. 4, pp. 3133-3142, Jul. 2018.
[27] Z. Yuan and M. R. Hesamzadeh, "Hierarchical coordination of TSO-DSO economic dispatch considering large-scale integration of distributed energy resources," *Applied Energy*, vol. 195, pp. 600-615, Jun. 2017.
[28] Z. Yuan and M. Reza Hesamzadeh, "A distributed economic dispatch mechanism to implement distribution locational marginal pricing," in *Proceedings of 2018 Power Systems Computation Conference (PSCC)*, Dublin, Ireland, Jun. 2018, pp. 1-7.
[29] Z. Yuan, S. Wogrin, and M. R. Hesamzadeh, "Towards the power synergy hub (PSHub): coordinating the energy dispatch of super grid by modified Benders decomposition," *Applied Energy*, vol. 205, pp. 1419-1434, Nov. 2017.
[30] Z. Yuan, "Convex optimal power flow based on second-order cone programming: models, algorithms and applications," Ph. D. dissertation, KTH Royal Institute of Technology, Stockholm, Sweden, 2018.
[31] Z. Yuan, M. R. Hesamzadeh, S. Wogrin *et al.* (2021, Aug.). Stochastic optimal operation of the VSC-MTDC system with FACTS devices to integrate wind power. [Online]. Available: https://arxiv. org/abs/2108. 12693
[32] Z. Yuan and M. Paolone, "Properties of convex optimal power flow model based on power loss relaxation," *Electric Power Systems Research*, vol. 186, p. 106414, Sept. 2020.
[33] J. Bezanson, A. Edelman, S. Karpinski *et al.* (2015, Jul.). Julia: a fresh approach to numerical computing. [Online]. Available: https://arxiv.org/pdf/1411.1607v4.pdf
[34] I. Dunning, J. Huchette, and M. Lubin, "Jump: a modeling language for mathematical optimization," *SIAM Review*, vol. 59, no. 2, pp. 295-320, Mar. 2017.
[35] U.S.-Canada Power System Outage Task Force. (2004, Apr.). Final report on the August 14, 2003 blackout in the United States and Canada: causes and recommendations. [Online]. Available: https://eta. lbl. gov/publications/final-report-august-14-2003-blackout
[36] A. Wachter and L. T. Biegler, "On the implementation of an interior-point filter line-search algorithm for large-scale nonlinear programming," *Mathematical Programming*, vol. 106, pp. 25-27, Mar. 2006.
[37] R. D. Zimmerman, C. E. Murillo-Sánchez, and R. J. Thomas, "MATPOWER: steady-state operations, planning, and analysis tools for power systems research and education," *IEEE Transactions on Power Systems*, vol. 26, no. 1, pp. 12-19, Jan. 2011.
[38] J. H. Chow, *Time-scale Modeling of Dynamic Networks with Applications to Power Systems*. Berlin: Springer-Verlag, 1982.
[39] University of Washington. (1999, Aug.). Power systems test case archive. [Online]. Available: http://www. ee. washington. edu/research/pstca/
[40] S. Fliscounakis, P. Panciatici, F. Capitanescu *et al.*, "Contingency ranking with respect to overloads in very large power systems taking into account uncertainty, preventive, and corrective actions," *IEEE Transactions on Power Systems*, vol. 28, no. 4, pp. 4909-4917, Nov. 2013.
[41] A. B. Birchfield, T. Xu, K. M. Gegner *et al.*, "Grid structural characteristics as validation criteria for synthetic networks," *IEEE Transactions on Power Systems*, vol. 32, no. 4, pp. 3258-3265, Jul. 2017.

Zhao Yuan received joint Ph.D. degree from KTH Royal Institute of Technology, Stokholm, Sweden, Comillas Pontifical University, Matrid, Spain, and Delft University of Technology, Delft, the Netherlands, in 2018. He proposed and proved the solution existence-and-uniqueness theorems of the convex optimal power flow model. He led the development of the energy management system of the 560 kWh/720 kVA battery energy storage system (BESS) on the Swiss Federal Institute of Technology Lausanne (EPFL) Campus, Lausanne, Switzerland, and co-developed the Smart Grid in Aigle, Switzerland. He worked as a Scientist at EPFL from 2019 to 2021. He is the Erasmus Munds Fellow of the European Commission. He is currently an Assistant Professor and the Head of the Electrical Power Systems Laboratory (EPS-Lab) at the University of Iceland, Reykjavík, Iceland. His research interests include power system, energy storage, renewable energy, electricity market and operations.